International Journal of Steel Structures
https://doi.org/10.1007/s13296-018-0018-x

Experimental and Analytical Study of Eccentrically Braced Frames Combined with High-Strength Steel

Shen Li[1] · YunHe Liu[1] · JianBo Tian[1]

Received: 24 February 2017 / Accepted: 13 November 2017

Abstract
In the structure of high-strength steel composite eccentrically braced steel frames (HSS–EBFs), the links and braces are made of Q345 steel, while the non-energy-dissipation segments (columns and beams) are made of high-strength steel (HSS). HSS reduces the cross-section of the members and increases the economic efficiency. Here, four groups of K-HSS–EBFs are designed by performance-based plastic design method in this paper, which includes 5-storey, 10-storey, 15-storey and 20-storey, and each group contain four different link length (900, 1000, 1100 and 1200 mm). The cyclic test loading was applied to 1:2 scale three-storey K-type HSS–EBFs (K-HSS–EBFs) with shear links to investigate their seismic performance. The results indicate that the as-prepared K-HSS–EBF structure exhibits excellent bearing capacity, ductility, and energy dissipation. We also find that the fracture of the link web in the second storey led to the degradation of the load-carrying capacity. The non-designated yield members remained in the elastic stage, whereas the links ultimately experience inelastic rotations, and thus dissipate the energy in the K-HSS–EBFs. Moreover, nonlinear pushover analyses and nonlinear dynamic analyses are conducted, and the loading capacity, link rotations, ductility, interstory drifts and failure mode under rare earthquake of all models are compared. The results indicate that K-HSS–EBFs with different link length have similar deformation characteristic and failure mode under pushover analysis or rare earthquakes, and the interstory drifts, link rotations and ductility of HSS–EBFs are increased with rising the link length.

Keywords High strength steel · Eccentrically braced frames · Seismic performance · Failure mode · Link · Ductility

1 Introduction

In the structural system of eccentrically braced frames (EBFs), axial forces are transferred to the column or brace via shear and bending in a beam segment named "link" (Hjelmstad and Popov 1982). Figure 1 presents four typical EBF configurations, where the link length is denoted by e. These frames have often been proposed as a less expensive and more valid alternative structure to the most commonly used moment-resisting frames (MRFs) and concentrically braced frames (CBFs), as EBFs could incorporate the advantages of both MRFs and CBFs. Indeed, as the presence of braces and links, EBFs are expected to have the characteristics of both high lateral stiffness and high energy dissipation capacity (Bosco and Rossi 2009; Wang et al. 2016; Lian et al. 2015; Dusicka et al. 2010). The links serve as the structural fuses, yielding under severe earthquake loading and dissipating energy while the other frame components remain elastic (Speicher and Iii 2016). Rules for fabricating EBFs suggest that non-energy-dissipating members should be designed by forces multiplied by the magnification coefficient (AISC341-10), which will lead to the oversized cross-sections of columns and beams, and thus making it hard to be used in practical engineering.

Also, the HSS exhibits a small yield-to-tensile ratio and weak plastic deformation capacity with the improvement of the strength (Azizinamimi and Barth 2004; Green and Sause 2002; Mans et al. 2001). To ensure the safety of the structures, which should have enough redundancy and plastic deformation capacity, steel in seismic areas are specified by the following norms for the seismic design of buildings (GB50011-2010): (1) The ratio of the measured yield stress values to the measured tensile strength should not be greater than 0.85. (2) The steel should have an apparently yielding

✉ Shen Li
lishen2861@163.com

[1] School of Civil Engineering and Architecture, Xi'an University of Technology, Xi'an 710048, People's Republic of China

Published online: 25 April 2018

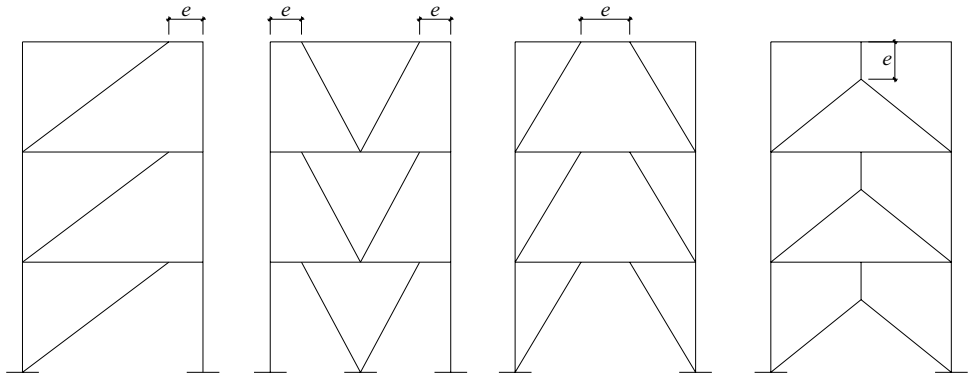

Fig. 1 EBF types

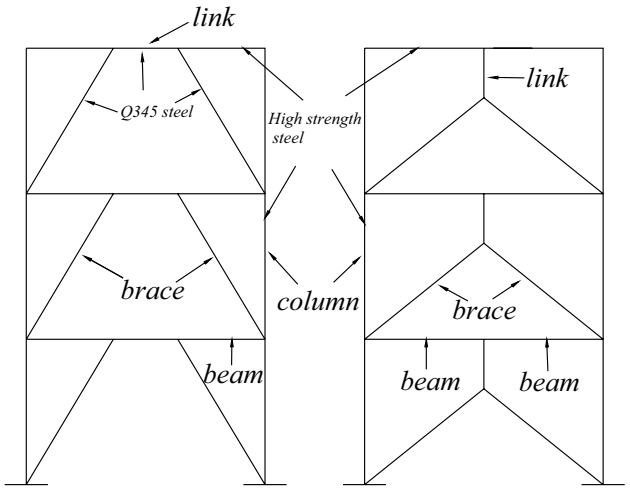

Fig. 2 Typical HSS–EBFs

platform, and the elongation should not be less than 20%. Therefore, these mandatory provisions limit the use of HSS in the seismic field.

To solve the above-mentioned problem, eccentrically braced dual systems which named EBFs with HSS combination (HSS–EBFs) have been proposed, where the links and braces are made of Q345 steel (with a specified nominal yield strength of 345 MPa), and other structural members are made of high-strength steel (HSS) (e.g., Q460 steel with the nominal yield strength of 460 MPa or Q690 steel with a nominal yield strength of 690 MPa). The goal of using HSS–EBFs is to reduce the steel consumption, and to improve the economic benefit. Figure 2 presents some examples of the typical HSS–EBFs. The HSS–EBF system exhibits superior plastic deformation and energy dissipation ability under rare earthquakes and contributes to the practical application of HSS in seismic zones due to the links use ordinary steel (yielding stress of less than 345 MPa) with better deformability than HSS. However, other members which using HSS (e.g., columns and beams) remain elastic or undergo partial yielding, while the links deform to dissipate energy sufficiently. Therefore, the yield-to-tensile ratio and elongation are not strict requirements for HSS.

In the related study, four K-type HSS–EBF specimens were tested at the Politehnica University of Timisoara in Romania (Dubina et al. 2008). These specimens used removable links fastened to beams using flush end-plate bolted connections. To investigate the seismic performance of HSS-EBFs, a half-scale three-storey one-bay K-type HSS–EBF (K-HSS–EBF) specimen with shear links was tested under cyclic loading, and four groups of K-HSS–EBFs are designed and analyzed by pushover and dynamic to research the seismic response.

2 Experimental Description

2.1 Specimen Overview

The design is characterized by a peak ground acceleration of 0.3 g with 10% probability of exceedance in a 50-year period and moderately firm ground conditions. The factor that reduces the elastic response spectrum to obtain the design spectrum is 2.8 in GB50011-2010. The alpha damping α and beta damping β are specified according to the damping ζ and fundamental frequencies of the structures. Moreover, damping of 4% is considered for the steel building with the structural height not exceeding 50 m and 3% for structural heights between 50 and 200 m according to the requirements of GB50011-2010. The designed frame was located on a firm rock (site class II in the Chinese code), and the design earthquake group is the first one. In the EBFs design, the seismic forces were calculated using the provision of GB50011-2010 according to seismic hazard., provisions of the GB50017-2003 code for the design of steel structures (GB50017-2003) and the AISC Seismic

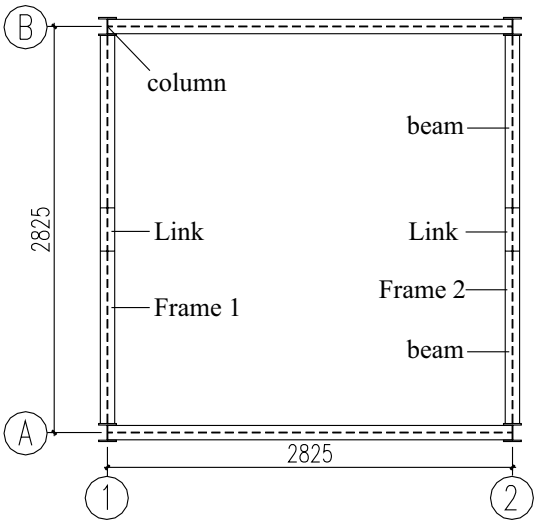

Fig. 3 Plan view of specimen

Provisions for Structural Steel Buildings (AISC341-10 2010) were used to design the steel members. A 5.0 kN/m^2 dead load and 2.0 kN/m^2 live load was considered in the first and second storey, and the third-storey dead load, live load, and snow load were deemed to be 6.0, 2.0, and 0.25 kN/m^2, respectively.

The plan view of the three-story test structure is shown in Fig. 3. The test structure was formed by two frames (1, 2) parallel to the loading direction and two frames (A, B) perpendicular to the loading direction. Frames 1 and 2 had an eccentric bracing system, which is described in the following conveniently. A half-scale was considered by the test site condition, loading capacity of the actuator. The frame elevations are also shown in Figs. 4 and 5. The prototype structure has one span of 2.825 m and one bay of 2.825 m, and three storeys of 1.8 m each, The links' length was of $e=350$ mm. Short links were chosen, which dissipate energy by yielding in shear. The ratio of e to the bay width (L) (e/L) is 0.124, ($\rho=0.964$, where $\rho=eV_p/M_p$ and M_p and V_p are the plastic moment and shear capacity of the link, respectively. $\rho=0.964<1.6$, the link is short (or shear yielding) in design according to the AISC341-10). In the test structure, the links and braces of the structures used Q345B steel with a nominal yield strength of 345 MPa, while the columns and beams used Q460C steel with a nominal yield strength of 460 MPa. Welded joints were used to connect the link to the beam and other joints in the test specimen. Furthermore, the link and beam had the same section in the specimen tested. However, different sections can be used for the link and beam in practical engineering because the strength of the steel used in the links is distinct from that in the beams. Moreover, the links can be removed after an earthquake because the members using HSS remain in elastic by constraining plastic deformations to the links. Full-depth web stiffeners are fabricated on

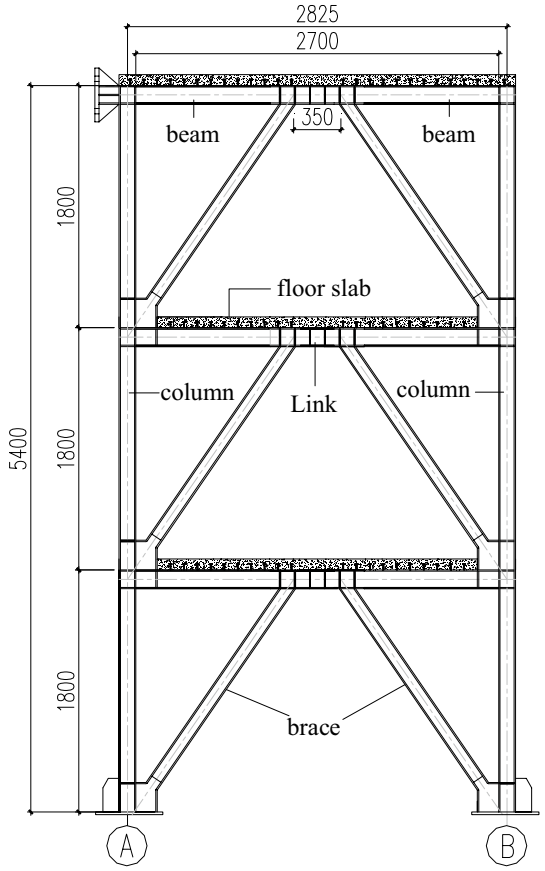

Fig. 4 Elevation view of specimen

both sides of the link web, with a spacing of 110 mm. The detailed member sections are listed in Table 1, where "H" refers to the welded H-shaped section, with section depth of h, flange width of b_f, web thickness of t_w, and flange thickness of t_f (in mm), see Fig. 6. The mechanical properties of the steel are presented in Table 2.

2.2 Details

Several fabrication details of the text structure should be explicated. First, the shear studs between the floor slab and beam were not used in the segment of links; consequently, composite slab does not affect the shear capacity of the links. Secondly, a butt-welding joint was adopted in the connection of link to beam, which is located on the ends of the links to avoid the force transferred from the brace. Meanwhile, the girders, which include link and beam, as a whole one, the beam and the concrete floor connected by the shear studs, so concrete floors with enough rigidity can restrict the lateral buckling in the links. Finally, the stress concentration of the brace joint can be eliminated by circular arc transition in the flange gusset plate. Figure 7 presents the corresponding details.

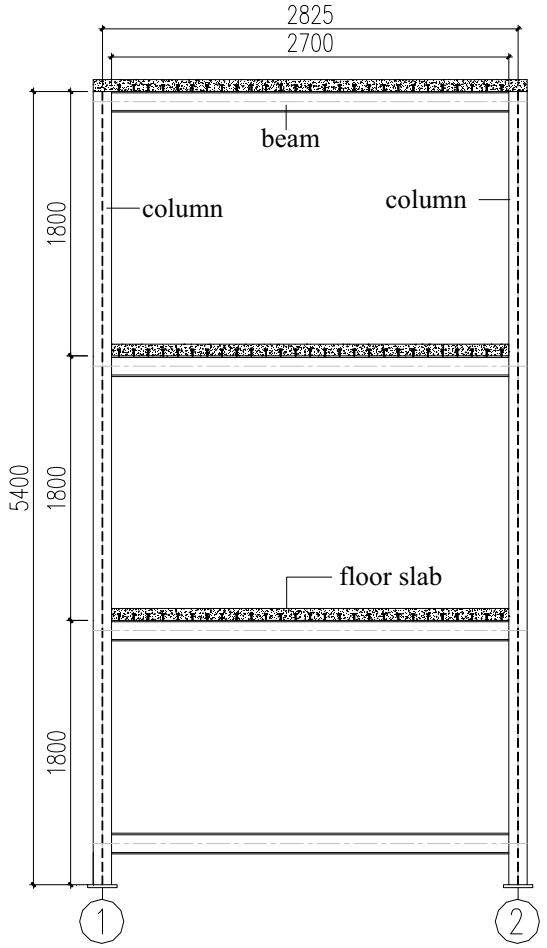

Fig. 5 Elevation view of specimen

Table 1 Member sizes for the specimen

Member	Section ($h \times b_f \times t_w \times t_f$)	Material
Column	H125 × 125 × 8 × 10	Q460C
Beam	H140 × 100 × 8 × 10	Q460C
Link	H140 × 100 × 6 × 10	Q345B
Brace	H100 × 100 × 6 × 10	Q345B

2.3 Experimental Setup and Loading Protocol

A representative value of the gravity load (1.0 × dead load + 0.5 × live load) was first applied to the structure by placing numerous sand bags on the first storey, second storey, and roof to achieve loads of 6.3, 6.3, and 7.1 kN/m^2, respectively.

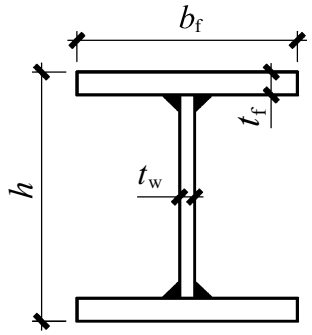

Fig. 6 Specimen sectional dimensions

Table 2 Mechanical properties of the steel

Steel	Q345B	Q345B	Q460C	Q460C
Thickness t (mm)	6.07	9.72	7.78	9.65
Yield stress f_y (MPa)	414.7	363.8	473.5	455.6
Ultimate strength f_u (MPa)	542.0	545.8	635.1	598.5
Elastic modulus E ($\times 10^5$ MPa)	2.11	2.01	2.12	1.96
Elongation ratio (%)	28.29	28.74	25.36	23.48

The horizontal cyclic loads were then applied to the test structure using two 1000-kN servo-actuators installed on the reaction wall. A typical experimental setup of quasi-static loading was used for the HSS–EBF specimen, as illustrated in Fig. 8.

Horizontal loads were applied with mixed force and displacement to the text structure in cycles. The loading protocol used for testing is depicted in Fig. 9. The test loads began with a load control: this loading protocol specifies one cycle at each of the control levels of 0.25F$_y$, 0.50F$_y$, 0.75F$_y$, and 1.0F$_y$ (F$_y$ is the estimation loading capacity of the specimen) until stiffness degradation could be obviously observed in the hysteretic curves of the test structure. The corresponding displacement was defined as the yield displacement (Δ_y). After several initial elastic cycles, the loading protocol requires increasing the applied yield displacement in increments of 0.5Δ_y, with three cycles of loading applied at each increment of displacement.

2.4 Measurement

For the test method, the structure was interfaced with the computer using actuators and displacement measuring transducers such that the response of the building to a given force

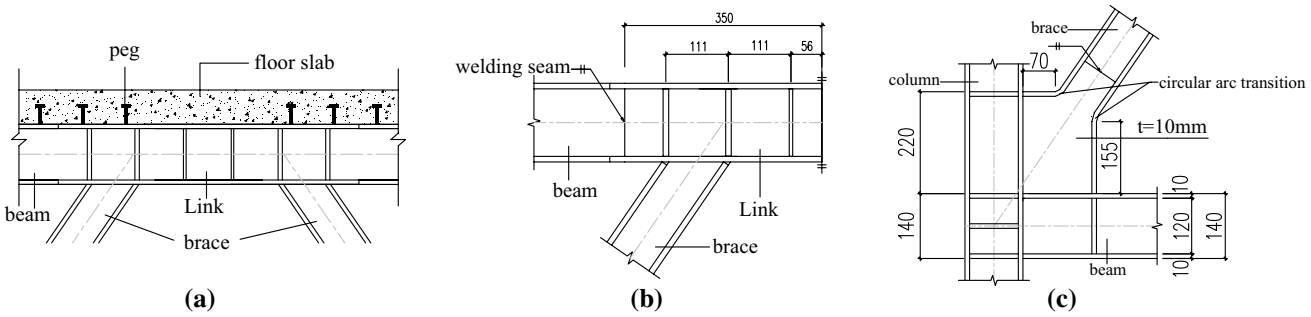

Fig. 7 Details of specimen. **a** No shear studs in link, **b** Connection between beam and link, **c** brace joint

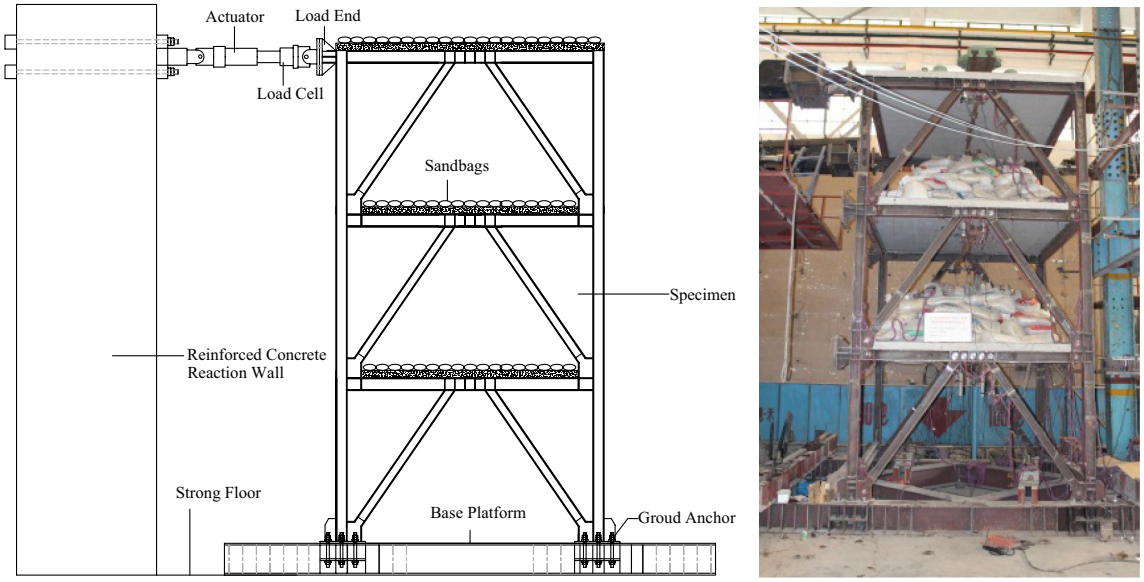

Fig. 8 Test setup

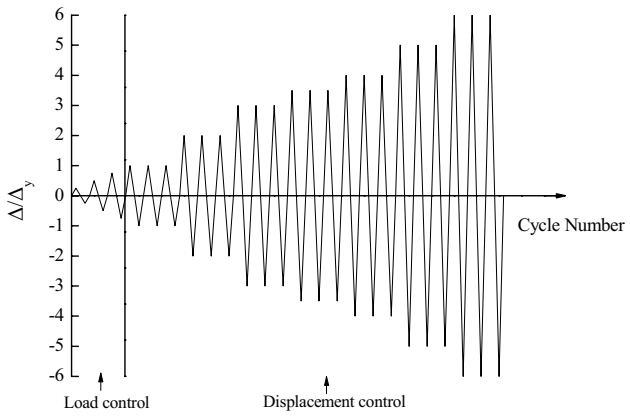

Fig. 9 Loading protocol

was self-controlled to provide excellent simulation (Mahin and Shing 1985; Okampto 1983).

Figures 10 and 11 show two types measuring instruments. The first type was linear variable displacement transducers (LVDTs) to acquire the horizontal displacement for each storey. These data were used to study the load–deformation relationship of the test structure, the drift–rotation relationship of the links, storey shear–drift relationship for each storey. The second type was strain gauges, which were installed in some higher-stress areas (e.g. link web, link flange, column-to-beam connections, column base) to get the principal stresses of the specimen.

Approximately 400 channels of the two types of data were collected for the test. The data included:

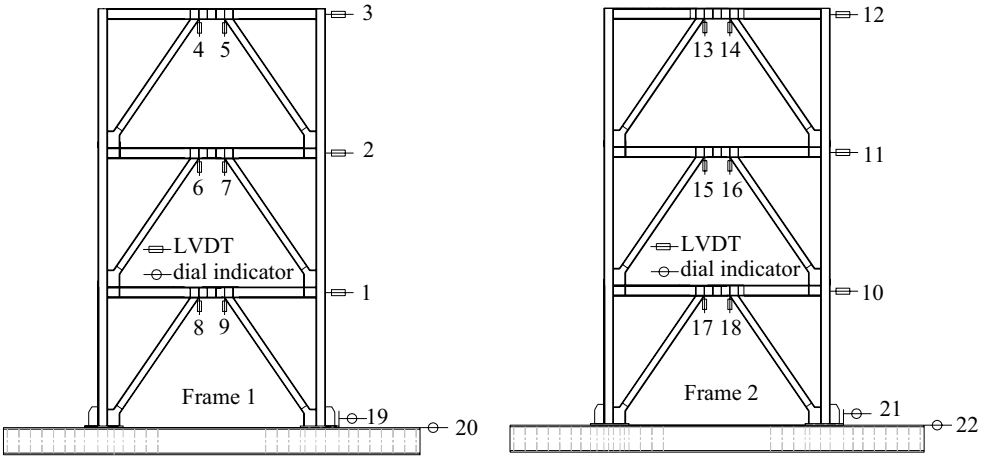

Fig. 10 Displacement measurement

Fig. 11 Strain measurement

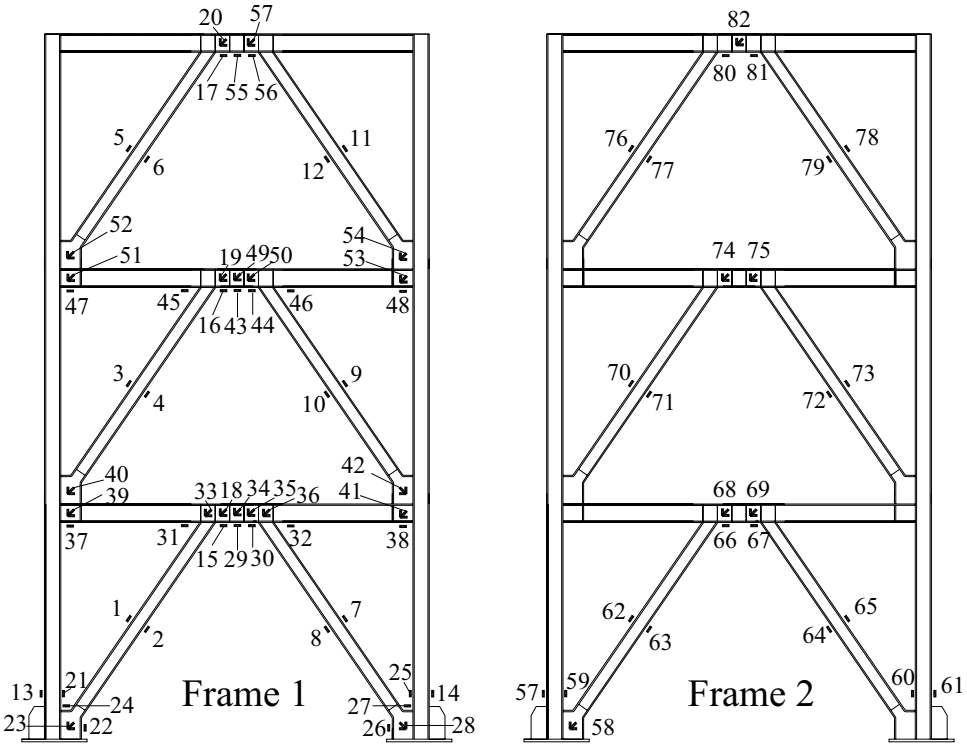

(1) Four groups of strain gauges were installed column bases in Frames 1 and 2. These data were used to determine the axial force, bending moments, and shear force in the column bases and to help observe the initiation of yielding.
(2) A total of 24 strain gauges were attached to the cross-bracing in Frame 1 and Frame 2 to estimate the forces in these members.
(3) Three groups of strain gauges were attached to the links in Frame 1, including flanges and webs. These data helped to detect the initiation and process of yielding. For comparison with Frame 1, strain gauges were similar installed to the links in Frame 2.
(4) Displacement transducers were attached in parallel at each storey to determine the storey drift. Two vertical displacement sensors were connected to the ends of each link to measure the rotation of the links.
(5) Additional strain gauges were installed to research local effects such as the brace-beam connection and the ends of beams.

3 Experimental Results and Analysis

3.1 Failure Process and Failure Mode

Two MTS servo-actuators were connected with Frames 1 and 2, which was controlled by the identical displacement after yielding. Therefore, the failure mode of Frame 1 was similar to that of Frame 2. The failure process of the K-HSS–EBF included four stages: the elastic stage, concrete floor cracking, inelastic shear deformation of the links, and the failure. First, the experimental phenomenon was not visible before yielding of the links. Then, significant yielding can be observe in the link web panel one after another at $1.0\Delta_y$ due to storey shear at each frame equal to the force generated by the servo-actuator. The lateral rigidity of the test specimen was reduced, as demonstrated by the hysteresis curves. There were gaps between the contact surfaces of the concrete floors and links because there were no shear studs in the links segment. Therefore, the links did not exhibit composite floor action. With the increment of displacement, the links' shear increased steadily, and diagonal cracks appeared symmetrically in the concrete floors in the segment of links at $1.5\Delta_y$. As one crack was generated in the push loading direction, another was generated upon reversal (Figs. 12a, 13a). Then, the shear deformation of the links was apparently observed, and the slab concrete continuously fell off in the region of links affected by shear until rebar exposed (Figs. 12b, 13b). At $3.0\Delta_y$, the link web of the second storey and roof initiated fractures at the fillet welds connecting the web stiffeners to the link flange

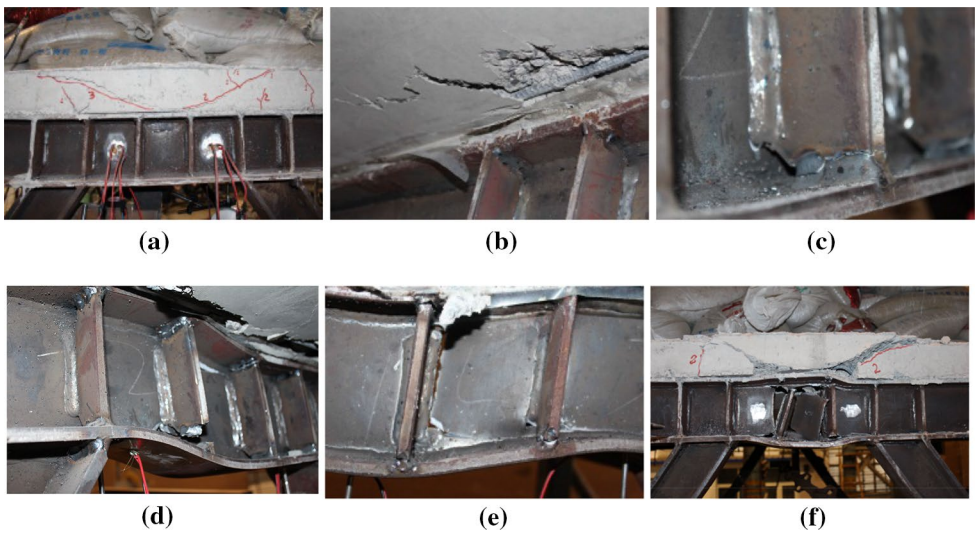

Fig. 12 Failure process of Frame 1. **a** Diagonal crack, **b** bare rebar, **c** weld crack, **d** stiffener fracture, **e** web broken, **f** web failure

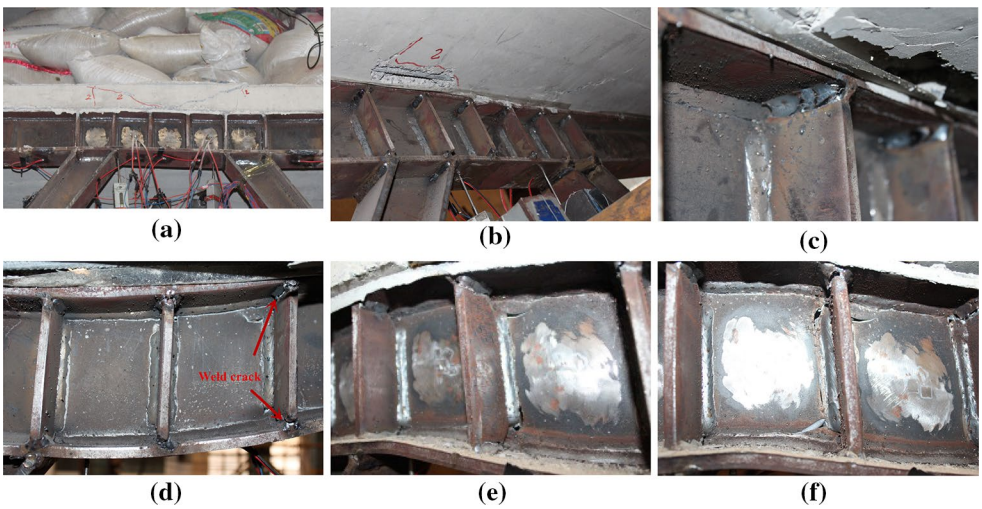

Fig. 13 Failure process of Frame 2. **a** Diagonal crack, **b** bare rebar, **c** weld crack, **d** weld crack, **e** web broken, **f** web failure

(Figs. 12c, d, 13c, d). The development of link web fracture led to strength degradation.

Finally, the shear broken of link web in the middle panel zone on the second storey was occured at $3.5\Delta_y$. The ruptures commonly develop in the vertical direction and perpendicular to the flanges, resulting in severe degradation of the strength. Figures 12e, f and 13e, f show the link web broken, which were the failure of test structure. The failure mode of K-HSS–EBFs was that all the links yielding to dissipate energy, and the other members remain in elastic. All inelastic activity was isolated to the links. The desired yielding mechanism for the HSS–EBFs was achieved.

3.2 Cyclic Behavior

Figure 14 illustrates the hysteretic response of the test specimen; the dashed and solid lines are representative of the responses of Frame 1 and Frame 2, respectively. The base shear for Frame 1 or Frame 2 is shown on the vertical coordinate, and the roof displacement is plotted on the horizontal coordinate. The hysteretic loop represents the energy dissipation of the specimen. Frame 1 and Frame 2 have stable and full hysteretic loops with no deterioration in stiffness before link web broken. The hysteresis curve of Frame 1 is similar to that of Frame 2. In the loading control, the hysteretic response loops exhibit a long and narrow shape before the links yield, and the specimen dissipates few energy. However in displacement control, with the increment of displacement, the hysteretic response loops expanded steadily. In the final, Frame 1 and Frame 2 reached to $3.5\Delta_y$ and $3.0\Delta_y$, respectively. The last hysteretic loop of Frame 2 became flat suddenly due to the fracture of the link web on the second-storey in Frame 2.

The backbone curves corresponding to the hysteresis curves of the specimen are presented in Fig. 15. The loading-carrying capacity of Frame 1 increased until the failure of the link similar to that of Frame 2. The slope of the Frame

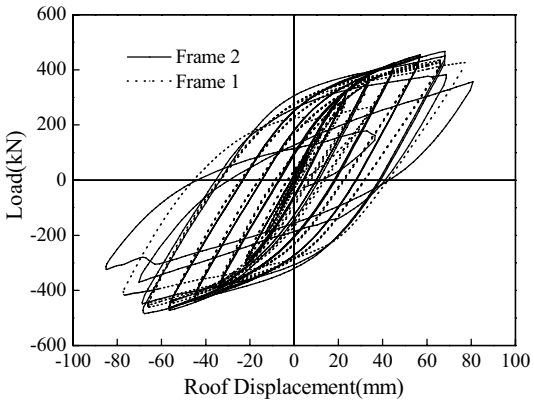

Fig. 14 Hysteresis curves

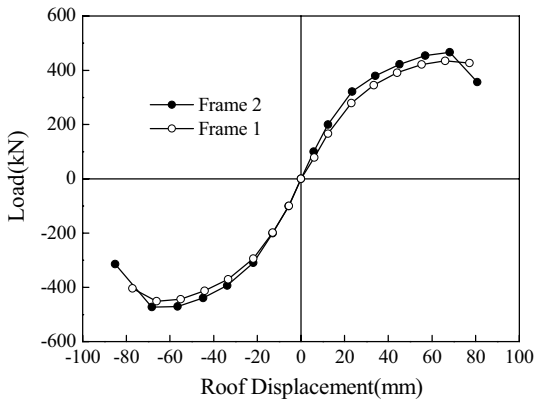

Fig. 15 Backbone curves

2 curve is slightly larger than that of frame 1 in the pull direction, whereas, in the push direction, they are almost equality. Therefore, the servo-actuators control the same displacement and the base shear of Frame 2 is greater than that of Frame 1 in the pull direction. Consequently, the link web broken in Frame 2 was prior to Frame 1. For the same reason, the bearing capacity of Frame 2 is less than Frame 1 at the last protocol level.

The energy dissipated by the test specimen, E, and the equivalent viscous damping coefficient, h_e, can be calculated as

$$E = S_{ABC} + S_{CDA} \tag{1}$$

$$h_e = \frac{S_{ABC} + S_{CDA}}{2\pi \times \left(S_{OBE} + S_{ODF}\right)}. \tag{2}$$

S_{ABC}, S_{CDA}, S_{OBE}, and S_{ODF} are shown in Fig. 16. In Table 3, the equivalent viscous damping coefficients of the test structures are listed. h_e increases steadily after the links yielding, which indicates that the energy dissipation capacity of the specimen continues to grow with increasing displacement. The E or h_e values of Frame 1 approximate to Frame

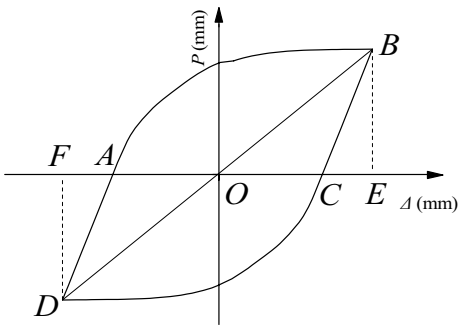

Fig. 16 Calculation of energy dissipation coefficient

Table 3 Energy dissipation of specimen

Frame 1				Frame 2			
Loading level		*E*/kJ	H_e	Loading level		*E*/kJ	H_e
1	100 kN	0.03	-	1	100 kN	0.08	-
2	200 kN	0.44	0.03	2	200 kN	0.51	0.03
3	$1.0\Delta_y$	2.24	0.06	3	$1.0\Delta_y$	2.87	0.06
4	$1.5\Delta_y$	8.01	0.11	4	$1.5\Delta_y$	9.98	0.12
5	$2.0\Delta_y$	17.65	0.16	5	$2.0\Delta_y$	20.61	0.17
6	$2.5\Delta_y$	30.30	0.20	6	$2.5\Delta_y$	35.65	0.22
7	$3.0\Delta_y$	44.83	0.24	7	$3.0\Delta_y$	52.31	0.26
8	$3.5\Delta_y$	56.21	0.28	8	$3.5\Delta_y$	37.17	0.21

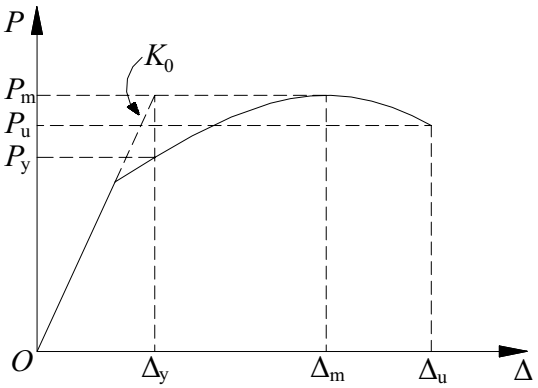

Fig. 17 Estimation of structural yield point

2 because of the similar deformation and failure process. Likewise, h_e decreases distinctly at the last loading level owing to the fracture of link web.

The calculation of the performance point data is illustrated in Fig. 17. K_0 is the elastic lateral stiffness; P_y and Δ_y are the yielding strength and yielding displacement, respectively; P_m and Δ_m are the maximum strength and maximum displacement, respectively; and P_u and Δ_u are the ultimate strength and ultimate displacement (Park 1988). The ultimate point is defined as the corresponding point of $0.85\times P_m$ or the failure point. The displacement ductility coefficient can be calculated as

$$\mu = \frac{\Delta_u}{\Delta_y}. \tag{3}$$

The behavior dates based on the backbone curves are listed in Table 4. θ_y, θ_m, and θ_u are the roof drift corresponding to Δ_y, Δ_m, and Δ_u, respectively. In both the pull and push directions, the behavior data of Frame 1 is similar to that of Frame 2. It is remarkable that Δ_y of Frame 1 in the pull direction is greater than the other; in other words, the lateral stiffness of Frame 1 in the pull direction is stronger than that of Frame 2, which led to the aforementioned failure mode. The equivalent viscous damping coeicient increased with the loading level is depicted in Fig. 18.

The peak stiffness of the specimen can be calculated as

$$K = \frac{|P^+| + |P^-|}{|\Delta^+| + |\Delta^-|}, \tag{4}$$

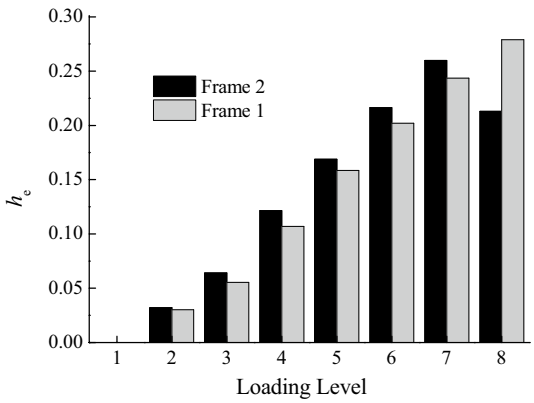

Fig. 18 Energy dissipation coefficient

Table 4 Performance index of specimen

Frame	Direction	Yield			Max			Failure			Lateral stiffness K_0/(kN mm^{-1})	Ductility μ
		Δ_y/mm	θ_y/%	F_y/kN	Δ_m/mm	θ_m/%	F_m/kN	Δ_u/mm	θ_u/%	F_u/kN		
Frame 2	Push	28.04	0.52	351.80	68.18	1.26	466.84	76.70	1.42	396.82	16.66	2.74
	Pull	28.47	0.53	361.50	68.28	1.26	472.58	76.50	1.42	401.69	16.59	2.69
Frame 1	Push	32.96	0.61	341.80	66.07	1.22	435.02	77.19	1.43	426.80	13.20	2.34
	Pull	26.53	0.49	328.80	66.12	1.22	451.08	77.20	1.43	404.08	16.70	2.91

where P^+ and P^- are the maximum lateral force in the positive and negative directions in the hysteretic loop, respectively, and Δ^+ and Δ^- are the maximum top storey displacements corresponding to the maximum lateral force. The stiffness degradation reflects the stiffness variation of the test structure. Figure 19 presents the stiffness degradation curves of the test frame given by Eq. (4). The initial peak stiffness of Frame 1 is less than that of Frame 2. However, the peak stiffness tendency of Frame 1 is an approach to of Frame 2. In the failure, the peak stiffness of Frame 1 is 5.38 kN mm^{-1}, approximately 35% of the elastic peak stiffness, whereas that of Frame 2 is 4.04 kN mm^{-1}, almost 23% of the elastic peak stiffness.

3.3 Storey Drift and Link Rotation

The maximum inelastic storey drift of the steel structure is 5% according to GB50011-2010, and the maximum plastic rotation of the shear link is 0.08 rad according to AISC341-10. However, the interstory drift and link rotation of the test specimen play a significant role in the discussion of seismic performance. Curves of storey drift versus storey shear are presented in Fig. 20. The storey drifts are approximately equivalence before link yielding, and the growth rate of interstorey drift in second-storey is fastest owing to the weakest storey lateral stiffness. The maximum storey drifts of Frame 1 and Frame 2 are 1/53 and 1/42, respectively. The curves of link rotation to storey drift are shown in Fig. 21. The relationship between the link rotation and storey drift exhibits a bilinear property, and the inflection point of the curves is corresponding with the yielding point of backbone curves, and the plastic rotation γ_p of the link is approximately equal to $\theta_p \times (L/e)$, where θ_p is the plastic drift of the frame. The maximum link rotation is 0.0815 rad, and eliminates inaccuracy value in the failure.

The hysteretic curves between interstory drift and storey shear of Frame 1 and Frame 2 are shown in Figs. 22 and 23. Each storey curves have the similar hysteresis characteristic. The first storey of structure dissipate the least energy because the base is rigidity, the storey lateral stiffness is the most of three. The second storey of the structure shows largest storey drift and full hysteresis loop, the shear capacity of the second storey of Frame 2 reduce dramatically before Frame 1, because the web broken of the second storey of Frame 2 occur earlier.

The relationship between link rotation and link shear are shown in Fig. 24, The horizontal and vertical coordinates are link rotations and V/V_p, respectively, where V is link shear, V_p is the plastic shear capacity of link, $V_p = 0.58 f_y h_0 t_w$. The curves present bilinear feature. Obviously, the link rotation and storey shear are in a straight line firstly due to all links are in the elastic, the link rotations are also small at this stage. After the link's web yielding, it's in a horizontal line shape, and the link rotations are grown without shear force increasing due to the link shear reached to plastic shear

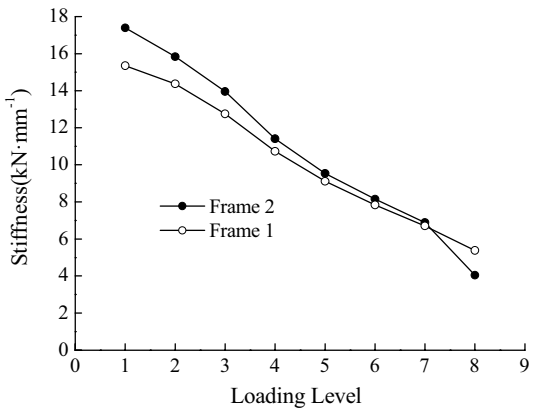

Fig. 19 Degradation of peak stiffness

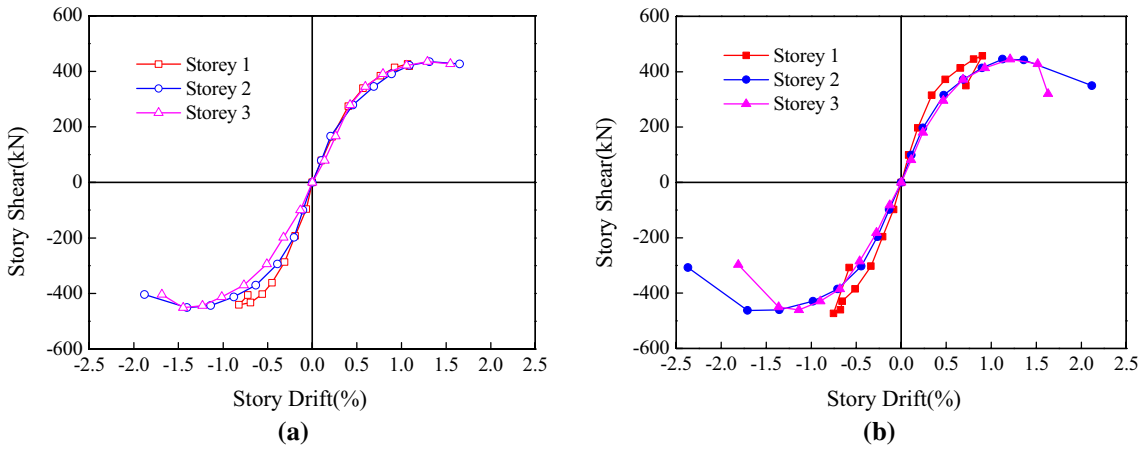

Fig. 20 Relationship between storey drift and storey shear. **a** Frame 1, **b** Frame 2

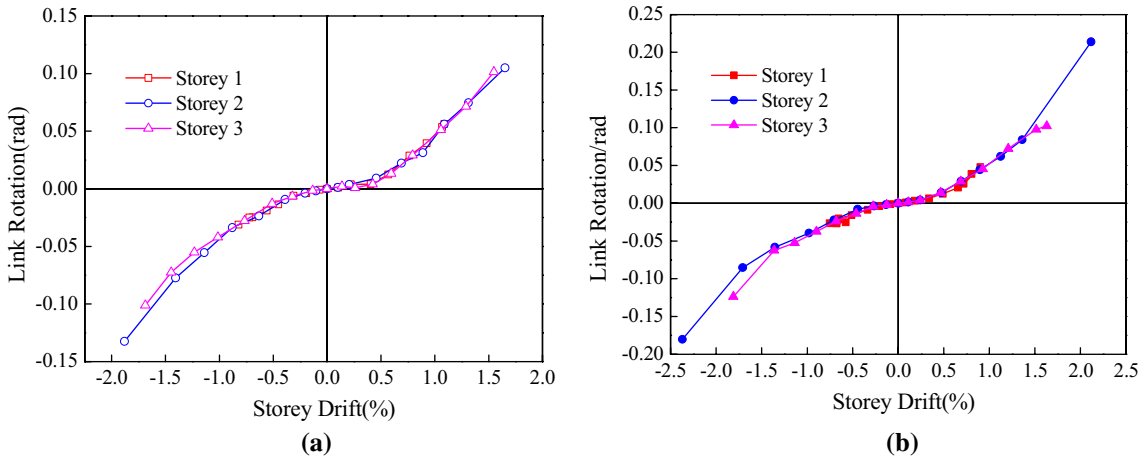

Fig. 21 Relationship between storey drift and link rotation. **a** Frame 1, **b** Frame 2

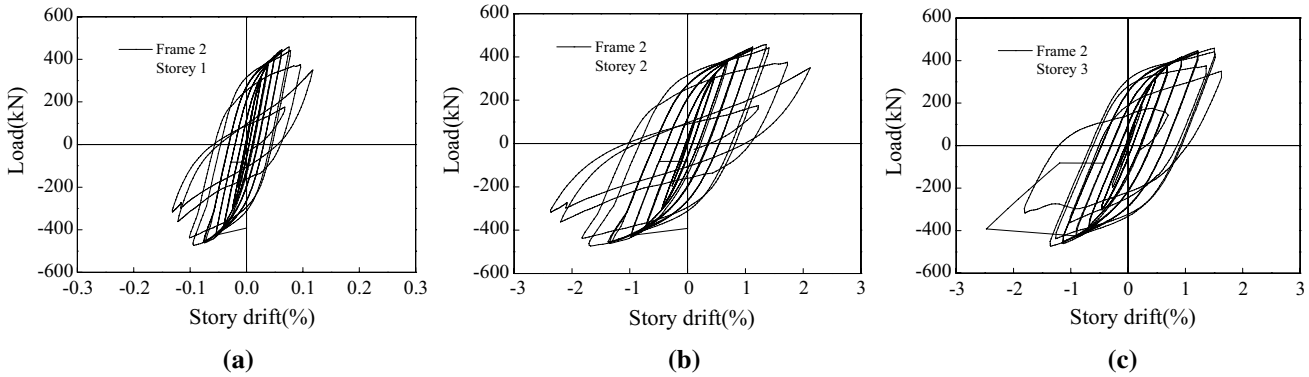

Fig. 22 Interstory hysteresis curves of Frame 2. **a** Storey 1, **b** storey 2, **c** storey 3

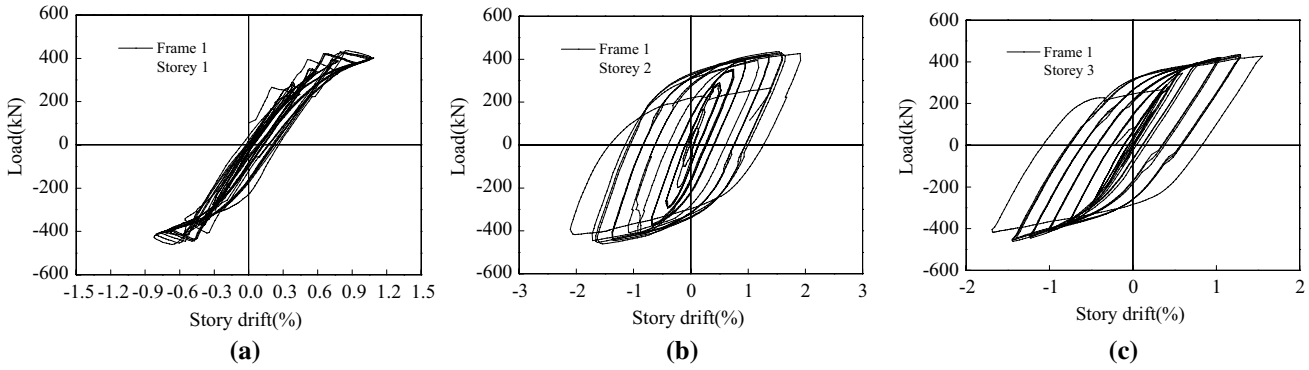

Fig. 23 Interstory hysteresis curves of Frame 1. **a** Storey 1, **b** storey 2, **c** storey 3

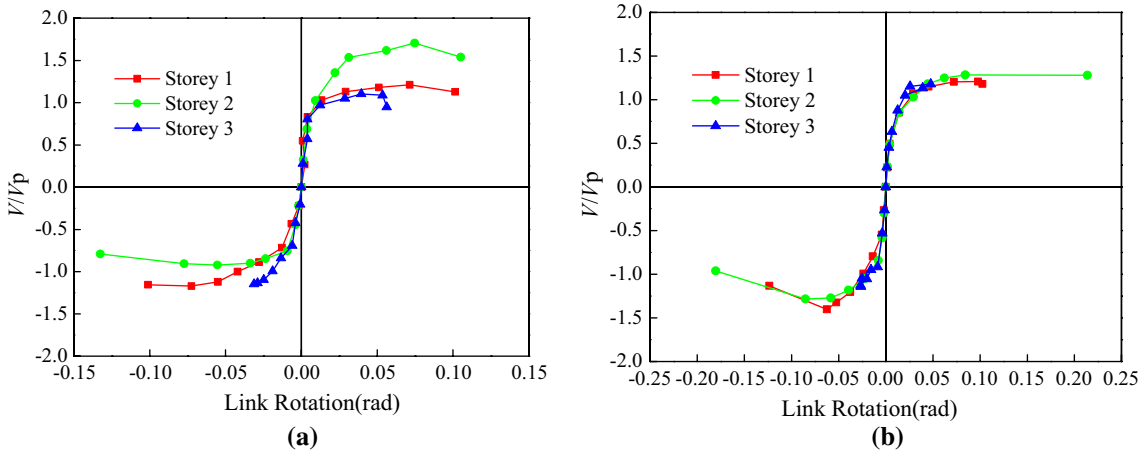

Fig. 24 Relationship between link rotation and shear. **a** Frame 1, **b** Frame 2

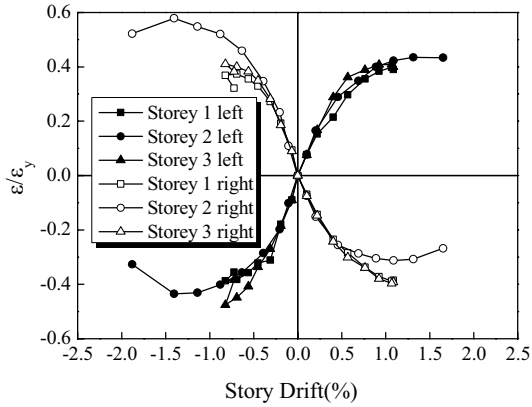

Fig. 25 Brace strain

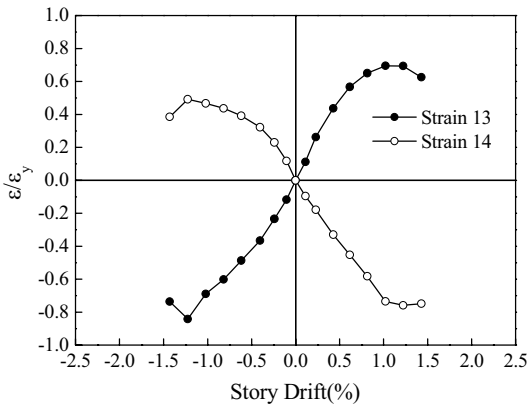

Fig. 26 Column base strain

capacity. The second-storey drift of Frame 2 grew in the last abruptly by reason of web broken.

3.4 Strain Analysis

As described in Sect. 2.3, the strain gauges were mainly measured in Frame 1. Therefore, the stress analysis of Frame 1 is discussed in the following. The relationship of the average strain (ε) value of the brace to the yielding strain (ε_y) with storey drift is presented in Fig. 25, where ε is the mean value of the top flange strain and bottom flange strain of the brace. For instance, the remaining ε of storey 1 is the average value of number 1 strain gauges and number 2 strain gauges. The average strain of the brace reflects the axial force of the brace and so indirectly indicates the shear of the links. The value of $\varepsilon/\varepsilon_y$ is smaller than 1.0, pointing out that the braces remained elastic during the testing. As observed in Fig. 26, the column base strain ($\varepsilon/\varepsilon_y$) is less than 1.0, demonstrating that the columns were not inelastic. The braces and columns remained elastic when the links yielded and failed, which contributed to seismic rehabilitation because the inelastic deformation of the test specimen was isolated in the links.

4 Finite Element Models

4.1 Designs

The site for the designs is characterized by the peak ground acceleration of 0.3 g with 10% probability of exceedance in a 50-year period and moderately firm ground conditions. The factor that reduces the elastic response spectrum to obtain the design spectrum is 2.8125 in GB50011-2010. The Alpha

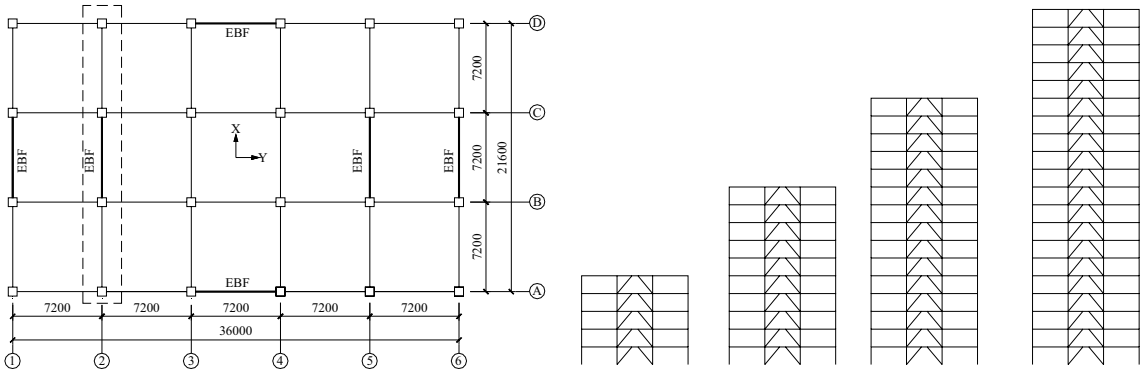

Fig. 27 Building plan and elevation views

damping α and Beta damping β were specified according to the damping ζ and the fundamental period of the structures. Moreover, damping of 4% is considered appropriate for a steel building with a structural height not exceeding 50 m, and 3% for structural heights between 50 and 200 m according to the requirements of GB50011-2010(in Chinese). In all design examples, the storey height is 3.6 m; there are five bays in the X-direction and three bays in the Y-direction. The span in both x-direction and that in y-direction were 7.2 m (see Fig. 27), the shear link lengths were 900, 1000, 1100 and 1200 mm in all designs for comparison. All links are designed to shear yielding (or short link). The constraints between columns of different stories were continuous and rigid connections were used between columns and beams in all design examples. Furthermore, the link had the same section of the beam connected at the same storey for EBFs. The frames located along the perimeter were designed to resist seismic loads and incorporated eccentric braces in the central span (see Fig. 27). The dead load for the floors and roofs were, respectively, 4.5 and 5.5 kN/m^2. The floor live load, roof live load, and snow load used 2, 0.5, and 0.25 kN/m^2, respectively. The detailed member sections are listed

Table 5 Member sections of 5 storey with e = 900

Storey	Beam	Link	Column	Brace	$\rho = eV_p/M_p$
5	H320×140×6×12	H320×140×6×12	B300×300×12	H200×200×8×12	1.43
4	H360×160×10×16	H410×160×8×14	B300×300×12	H220×220×8×12	1.35
3	H400×180×10×16	H430×180×10×16	B350×350×12	H240×240×8×12	1.31
2	H450×180×10×16	H490×180×10×16	B400×400×12	H260×260×10×16	1.27
1	H470×180×10×16	H520×180×10×16	B400×400×12	H260×260×10×16	1.24

Table 6 Member sections of 5 storey with e = 1000

Storey	Beam	Link	Column	Brace	$\rho = eV_p/M_p$
5	H320×140×6×10	H300×150×6×12	B300×300×12	H200×200×8×12	1.53
4	H330×150×10×16	H460×200×6×12	B300×300×12	H220×220×8×12	1.12
3	H370×180×10×16	H460×200×8×14	B350×350×12	H240×240×8×12	1.24
2	H400×180×10×16	H430×200×10×16	B400×400×12	H260×260×10×16	1.34
1	H430×180×10×16	H460×200×10×16	B400×400×12	H260×260×10×16	1.32

Table 7 Member sections of 5 storey with e = 1100

Storey	Beam	Link	Column	Brace	$\rho = eV_p/M_p$
5	H320×120×6×10	H300×150×5×12	B300×300×12	H200×200×8×12	1.43
4	H390×180×6×10	H420×200×6×12	B300×300×12	H220×220×8×12	1.25
3	H370×180×8×14	H410×200×8×14	B350×350×12	H240×240×8×12	1.39
2	H410×180×8×14	H390×200×10×16	B400×400×12	H240×240×8×12	1.51
1	H430×180×8×14	H410×200×10×16	B400×400×12	H240×240×8×12	1.49

Table 8 Member sections of 5 storey with e = 1200

Storey	Beam	Link	Column	Brace	$\rho = eV_p/M_p$
5	H300×120×6×10	H300×150×5×12	B300×300×12	H200×200×8×12	1.57
4	H350×150×6×12	H380×180×6×12	B300×300×12	H220×220×8×12	1.51
3	H380×150×8×14	H380×220×8×14	B350×350×12	H240×240×8×12	1.43
2	H420×150×8×14	H430×220×8×14	B400×400×12	H240×240×8×12	1.40
1	H440×150×8×14	H450×220×8×14	B400×400×12	H240×240×8×12	1.38

Table 9 Member sections of 10 storey with e = 900

Storey	Beam	Link	Column	Brace	$\rho = eV_p/M_p$
10	H300×150×8×14	H300×150×8×14	B300×300×12	H220×220×10×16	1.13
9	H370×150×10×16	H370×150×10×16	B350×350×12	H220×220×10×16	1.11
8	H490×180×10×16	H490×180×10×16	B400×400×16	H240×240×12×18	1.02
7	H500×200×12×18	H500×200×12×18	B400×400×16	H240×240×12×18	1.07
6	H570×200×12×18	H570×200×12×18	B450×450×20	H260×260×12×18	1.03
5	H540×240×14×20	H540×240×14×20	B450×450×20	H280×280×12×18	1.08
4	H580×240×14×20	H580×240×14×20	B500×500×20	H280×280×12×18	1.07
3	H610×240×14×20	H610×240×14×20	B500×500×20	H280×280×12×18	1.05
2	H630×240×14×20	H630×240×14×20	B580×580×25	H280×280×12×18	1.05
1	H640×240×14×20	H640×240×14×20	B580×580×25	H280×280×12×18	1.04

Table 10 Member sections of 10 storey with e = 1000

Storey	Beam	Link	Column	Brace	$\rho = eV_p/M_p$
10	H330×150×6×12	H340×160×6×12	B300×300×12	H200×200×10×16	1.41
9	H420×200×6×12	H420×200×8×14	B350×350×12	H200×200×10×16	1.26
8	H400×200×10×16	H450×200×10×16	B350×350×16	H240×240×10×16	1.33
7	H460×200×10×16	H530×250×10×16	B350×350×16	H240×240×10×16	1.08
6	H480×220×10×16	H500×200×12×18	B400×400×20	H260×260×12×18	1.15
5	H520×200×10×16	H550×250×12×18	B400×400×20	H260×260×12×18	1.12
4	H490×220×12×18	H580×250×12×18	B500×500×20	H260×260×12×18	1.11
3	H510×220×12×18	H610×250×12×18	B500×500×20	H260×260×12×18	1.09
2	H520×220×12×18	H630×250×12×18	B590×590×22	H260×260×12×18	1.08
1	H530×220×12×18	H640×250×12×18	B590×590×22	H260×260×12×18	1.08

Table 11 Member sections of 10 storey with e = 1100

Storey	Beam	Link	Column	Brace	$\rho = eV_p/M_p$
10	H300×150×6×12	H310×180×6×12	B300×300×12	H200×200×10×16	1.43
9	H450×150×6×12	H380×180×8×14	B350×350×12	H200×200×10×16	1.54
8	H410×200×8×14	H490×220×10×16	B350×350×16	H240×240×10×16	1.25
7	H470×200×8×14	H470×220×10×16	B350×350×16	H240×240×10×16	1.34
6	H440×220×10×16	H530×250×10×16	B400×400×20	H260×260×10×16	1.19
5	H470×220×10×16	H580×250×10×16	B400×400×20	H260×260×10×16	1.16
4	H500×220×10×16	H530×250×12×18	B480×480×20	H260×260×10×16	1.25
3	H520×220×10×16	H550×250×12×18	B480×480×20	H260×260×10×16	1.23
2	H530×220×10×16	H570×250×12×18	B550×550×20	H260×260×12×18	1.22
1	H540×220×10×16	H570×250×12×18	B550×550×20	H260×260×12×18	1.22

Table 12 Member sections of 10 storey with e = 1200

Storey	Beam	Link	Column	Brace	$\rho = eV_p/M_p$
10	H310×150×6×10	H320×150×5×12	B300×300×12	H200×200×10×16	1.55
9	H400×160×6×12	H440×200×6×12	B350×350×12	H200×200×10×16	1.35
8	H400×180×8×14	H440×200×8×14	B350×350×16	H220×220×10×16	1.50
7	H440×200×8×14	H520×250×8×14	B350×350×16	H220×220×10×16	1.21
6	H430×200×10×16	H480×240×10×16	B400×400×16	H240×240×10×16	1.37
5	H460×200×10×16	H520×250×10×16	B400×400×16	H240×240×10×16	1.30
4	H480×200×10×16	H560×250×10×16	B480×480×20	H250×250×10×16	1.28
3	H500×200×10×16	H580×250×10×16	B480×480×20	H250×250×10×16	1.27
2	H510×200×10×16	H600×250×10×16	B520×520×20	H250×250×10×16	1.26
1	H520×200×10×16	H610×250×10×16	B520×520×20	H250×250×10×16	1.25

Table 13 Member sections of 15 storey with e = 900

Storey	Beam	Link	Column	Brace	$\rho = eV_p/M_p$
15	H330×150×8×14	H370×180×6×12	B250×250×10	H200×200×10×16	1.14
14	H410×200×8×14	H370×180×10×16	B300×300×12	H220×220×10×16	1.35
13	H450×200×10×16	H470×200×10×16	B300×300×12	H240×240×10×16	1.18
12	H510×200×10×16	H560×240×10×16	B350×350×16	H260×260×10×16	0.99
11	H520×200×12×18	H540×240×12×18	B400×400×16	H260×260×10×16	1.05
10	H530×220×12×18	H590×240×12×18	B450×450×18	H280×280×12×18	1.02
9	H560×220×12×18	H560×240×14×20	B500×500×20	H280×280×12×18	1.07
8	H520×240×14×20	H590×240×14×20	B550×550×20	H300×300×12×18	1.06
7	H540×240×14×20	H620×240×14×20	B550×550×20	H300×300×12×18	1.04
6	H550×240×14×20	H640×240×14×20	B600×600×25	H300×300×12×18	1.04
5	H570×240×14×20	H660×240×14×20	B600×600×25	H300×300×12×18	1.03
4	H580×240×14×20	H680×240×14×20	B700×700×30	H300×300×12×18	1.02
3	H570×250×14×20	H690×240×14×20	B700×700×30	H300×300×12×18	1.01
2	H580×250×14×20	H700×240×14×20	B750×750×30	H300×300×12×18	1.01
1	H580×250×14×20	H710×240×14×20	B750×750×30	H300×300×12×18	1.00

Table 14 Member sections of 15 storey with e = 1000

Storey	Beam	Link	Column	Brace	$\rho = eV_p/M_p$
15	H350×150×6×12	H330×160×6×12	B250×250×10	H200×200×10×16	1.42
14	H400×180×8×14	H400×200×8×14	B300×300×12	H200×200×10×16	1.27
13	H410×200×10×16	H520×250×8×14	B300×300×12	H220×220×10×16	1.01
12	H470×200×10×16	H500×250×10×16	B350×350×16	H240×240×10×16	1.09
11	H520×200×10×18	H570×250×10×16	B350×350×16	H260×260×10×16	1.06
10	H480×220×12×18	H530×250×12×18	B400×400×16	H260×260×12×18	1.13
9	H510×220×12×18	H570×250×12×18	B450×450×20	H260×260×12×18	1.11
8	H540×220×12×18	H610×250×12×18	B500×500×20	H280×280×12×18	1.09
7	H560×220×12×18	H640×250×12×18	B500×500×20	H280×280×12×18	1.08
6	H580×220×12×18	H580×250×14×20	B550×550×25	H280×280×12×18	1.15
5	H530×200×12×18	H600×250×14×20	B550×550×25	H280×280×12×18	1.14
4	H560×220×14×20	H610×250×14×20	B630×630×25	H280×280×12×18	1.13
3	H570×220×14×20	H620×250×14×20	B630×630×25	H280×280×12×18	1.13
2	H570×220×14×20	H630×250×14×20	B680×680×28	H280×280×12×18	1.12
1	H580×220×14×20	H640×250×14×20	B680×680×28	H280×280×12×18	1.12

Table 15 Member sections of 15 storey with e = 1100

Storey	Beam	Link	Column	Brace	$\rho = eV_p/M_p$
15	H320×150×6×12	H310×160×6×12	B250×250×10	H200×200×10×16	1.58
14	H400×150×8×14	H470×200×6×12	B300×300×12	H200×200×10×16	1.22
13	H420×200×8×14	H470×200×8×14	B300×300×12	H220×220×10×16	1.35
12	H430×200×10×16	H550×250×8×14	B350×350×16	H220×220×10×16	1.10
11	H480×200×10×16	H510×250×10×16	B350×350×16	H240×240×10×16	1.20
10	H490×220×10×16	H560×250×10×16	B400×400×16	H260×260×10×16	1.17
9	H470×200×12×18	H610×250×10×16	B450×450×20	H260×260×10×16	1.15
8	H500×200×12×18	H550×250×12×18	B500×500×20	H260×260×12×18	1.23
7	H520×220×12×18	H580×250×12×18	B500×500×20	H260×260×12×18	1.22
6	H540×220×12×18	H600×250×12×18	B550×550×25	H260×260×12×18	1.21
5	H550×220×12×18	H620×250×12×18	B550×550×25	H260×260×12×18	1.20
4	H560×220×12×18	H640×250×12×18	B620×620×25	H260×260×12×18	1.19
3	H570×220×12×18	H650×250×12×18	B620×620×25	H260×260×12×18	1.18
2	H580×220×12×18	H660×250×12×18	B680×680×25	H260×260×12×18	1.18
1	H580×220×12×18	H660×250×12×18	B680×680×25	H260×260×12×18	1.18

Table 16 Member sections of 15 storey with e = 1200

Storey	Beam	Link	Column	Brace	$\rho = eV_p/M_p$
15	H320×150×6×10	H320×160×5×12	B250×250×10	H200×200×10×16	1.47
14	H400×150×8×12	H430×200×6×12	B300×300×12	H200×200×10×16	1.36
13	H420×200×8×12	H430×200×8×12	B300×300×12	H220×220×10×16	1.35
12	H400×200×10×16	H500×230×8×16	B350×350×16	H220×220×10×16	1.17
11	H440×200×10×16	H470×230×10×18	B350×350×16	H240×240×10×16	1.29
10	H480×200×10×16	H510×250×10×18	B400×400×16	H260×260×10×16	1.19
9	H460×200×12×18	H550×250×10×18	B450×450×20	H260×260×10×16	1.17
8	H480×200×12×18	H500×250×12×20	B500×500×20	H260×260×12×18	1.27
7	H500×200×12×18	H530×250×12×20	B500×500×20	H260×260×12×18	1.25
6	H520×200×12×18	H550×250×12×20	B550×550×25	H260×260×12×18	1.24
5	H530×200×12×18	H570×250×12×20	B550×550×25	H260×260×12×18	1.23
4	H540×200×12×18	H580×250×12×20	B600×600×25	H260×260×12×18	1.23
3	H550×200×12×18	H590×250×12×20	B600×600×25	H260×260×12×18	1.22
2	H560×200×12×18	H600×250×12×20	B650×650×25	H260×260×12×18	1.22
1	H570×200×12×18	H610×250×12×20	B650×650×25	H260×260×12×18	1.21

in Tables 5, 6, 7, 8, 9, 10, 11, 12, 13, 14, 15, 16, 17, 18, 19, 20, in which 'H' refers to the welded H-shaped section. The H-section's accompanying numbers are section depth h, flange width b_f, web thickness t_w, and flange thickness t_f, respectively. 'B' refers to the box section and the accompanying numbers are section depth h, section width b and wall thickness t, respectively, with a unit of mm. Links and braces of structures used steel Q345 ($f_y = 345$ MPa) while other structural members used steel Q460 ($f_y = 460$ MPa)

4.2 Member Sections

Member sections of the EBFs are designed based on the performance-based plastic design (PBPD) method according to the paper by Chao and Goel 2014, the designations of all buildings are summarized in Table 5, 6, 7, 8, 9, 10, 11, 12, 13, 14, 15, 16, 17, 18, 19, 20.

Nonlinear static pushover analysis and dynamic analysis were conducted to investigate the behaviour of the sample

Table 17 Member sections of 20 storey with e = 900

Storey	Beam	Link	Column	Brace	$\rho = eV_p/M_p$
20	H370×150×8×14	H390×160×6×12	B300×300×12	H200×200×10×16	1.24
19	H450×200×8×14	H460×200×8×14	B300×300×12	H220×220×10×16	1.11
18	H490×200×10×16	H480×200×10×16	B350×350×14	H240×240×10×16	1.18
17	H560×200×10×16	H570×250×10×16	B350×350×14	H240×240×10×16	0.96
16	H560×200×12×18	H550×250×12×18	B400×400×18	H260×260×10×16	1.01
15	H540×250×12×18	H600×250×12×18	B400×400×18	H280×280×12×18	0.99
14	H570×250×12×18	H650×250×12×18	B450×450×18	H280×280×12×18	0.97
13	H560×250×14×20	H600×250×14×20	B450×450×18	H280×280×12×18	1.02
12	H580×250×14×20	H640×250×14×20	B500×500×20	H300×300×12×18	1.01
11	H600×250×14×20	H670×250×14×20	B500×500×20	H300×300×14×20	0.99
10	H620×250×14×20	H690×250×14×20	B550×550×22	H300×300×14×20	0.98
9	H640×250×14×20	H720×250×14×20	B550×550×22	H300×300×14×20	0.97
8	H650×250×14×20	H740×250×14×20	B650×650×26	H300×300×14×20	0.96
7	H670×250×14×20	H670×250×16×22	B650×650×26	H300×300×14×20	1.02
6	H680×250×14×20	H680×250×16×22	B700×700×30	H300×300×14×20	1.01
5	H690×250×14×20	H700×250×16×22	B700×700×30	H340×340×16×22	1.01
4	H690×250×14×20	H710×250×16×22	B800×800×30	H340×340×16×22	1.00
3	H700×250×14×20	H710×250×16×22	B800×800×30	H340×340×16×22	1.00
2	H700×250×14×20	H720×250×16×22	B850×850×30	H340×340×16×22	1.00
1	H710×250×14×20	H720×250×16×22	B850×850×30	H340×340×16×22	1.00

Table 18 Member sections of 20 storey with e = 1000

Storey	Beam	Link	Column	Brace	$\rho = eV_p/M_p$
20	H340×150×8×14	H350×180×6×12	B300×300×12	H200×200×10×16	1.28
19	H420×200×8×14	H420×200×8×14	B300×300×12	H220×220×10×16	1.26
18	H460×200×10×16	H440×200×10×16	B350×350×14	H240×240×10×16	1.33
17	H520×200×10×16	H510×200×10×16	B350×350×14	H240×240×10×16	1.29
16	H520×200×12×18	H500×240×12×18	B400×400×18	H260×260×10×16	1.18
15	H540×220×12×18	H540×240×12×18	B400×400×18	H280×280×12×18	1.16
14	H570×220×12×18	H590×240×12×18	B450×450×18	H280×280×12×18	1.14
13	H530×240×14×20	H550×240×14×20	B450×450×18	H280×280×12×18	1.20
12	H550×240×14×20	H580×240×14×20	B500×500×20	H300×300×12×18	1.18
11	H570×240×14×20	H600×240×14×20	B500×500×20	H300×300×14×20	1.17
10	H590×240×14×20	H630×240×14×20	B550×550×22	H300×300×14×20	1.16
9	H600×240×14×20	H650×240×14×20	B550×550×22	H300×300×14×20	1.14
8	H620×240×14×20	H670×240×14×20	B650×650×26	H300×300×14×20	1.13
7	H630×240×14×20	H610×260×16×22	B650×650×26	H300×300×14×20	1.13
6	H640×240×14×20	H620×260×16×22	B700×700×30	H300×300×14×20	1.13
5	H650×240×14×20	H630×260×16×22	B700×700×30	H340×340×16×22	1.12
4	H660×240×14×20	H640×260×16×22	B800×800×30	H340×340×16×22	1.12
3	H660×240×14×20	H650×260×16×22	B800×800×30	H340×340×16×22	1.11
2	H670×240×14×20	H660×260×16×22	B850×850×30	H340×340×16×22	1.11
1	H670×240×14×20	H660×260×16×22	B850×850×30	H340×340×16×22	1.11

Table 19 Member sections of 20 storey with e = 1100

Storey	Beam	Link	Column	Brace	$\rho = eV_p/M_p$
20	H360×150×6×12	H320×200×6×12	B300×300×12	H200×200×10×16	1.30
19	H400×200×8×14	H490×240×6×12	B300×300×12	H220×220×10×16	1.05
18	H420×200×10×16	H480×240×8×14	B350×350×14	H240×240×10×16	1.17
17	H480×200×10×16	H570×250×8×14	B350×350×14	H240×240×10×16	1.09
16	H530×200×10×16	H530×250×10×16	B400×400×18	H260×260×10×16	1.19
15	H510×250×10×16	H580×280×10×16	B400×400×18	H280×280×12×18	1.07
14	H540×250×10×16	H630×280×10×16	B450×450×18	H280×280×12×18	1.05
13	H520×250×12×18	H570×280×12×18	B450×450×18	H280×280×12×18	1.12
12	H540×250×12×18	H600×280×12×18	B500×500×20	H300×300×12×18	1.11
11	H560×250×12×18	H630×280×12×18	B500×500×20	H300×300×14×20	1.10
10	H580×250×12×18	H660×280×12×18	B550×550×22	H300×300×14×20	1.08
9	H600×250×12×18	H680×280×12×18	B550×550×22	H300×300×14×20	1.08
8	H610×250×12×18	H610×280×14×20	B650×650×26	H300×300×14×20	1.15
7	H620×250×12×18	H630×280×14×20	B650×650×26	H300×300×14×20	1.14
6	H630×250×12×18	H640×280×14×20	B700×700×30	H300×300×14×20	1.13
5	H640×250×12×18	H650×280×14×20	B700×700×30	H340×340×16×22	1.13
4	H650×250×12×18	H660×280×14×20	B800×800×30	H340×340×16×22	1.12
3	H660×250×12×18	H670×280×14×20	B800×800×30	H340×340×16×22	1.12
2	H660×250×12×18	H670×280×14×20	B850×850×30	H340×340×16×22	1.12
1	H660×250×12×18	H680×280×14×20	B850×850×30	H340×340×16×22	1.11

Table 20 Member sections of 20 storey with e = 1200

Storey	Beam	Link	Column	Brace	$\rho = eV_p/M_p$
20	H330×150×6×12	H350×160×5×12	B300×300×12	H200×200×10×16	1.45
19	H410×200×6×12	H450×200×6×12	B300×300×12	H220×220×10×16	1.34
18	H440×200×8×14	H440×200×8×14	B350×350×14	H240×240×10×16	1.50
17	H500×200×8×14	H520×240×8×14	B350×350×14	H240×240×10×16	1.25
16	H470×220×10×16	H480×240×10×16	B400×400×18	H260×260×10×16	1.37
15	H510×220×10×16	H530×240×10×16	B400×400×18	H280×280×12×18	1.34
14	H540×220×10×16	H490×240×12×18	B450×450×18	H280×280×12×18	1.43
13	H490×240×12×18	H520×240×12×18	B450×450×18	H280×280×12×18	1.41
12	H510×240×12×18	H550×240×12×18	B500×500×20	H300×300×12×18	1.39
11	H530×240×12×18	H580×240×12×18	B500×500×20	H300×300×14×20	1.37
10	H550×240×12×18	H600×260×12×18	B550×550×22	H300×300×14×20	1.28
9	H570×240×12×18	H540×260×14×20	B550×550×22	H300×300×14×20	1.36
8	H580×240×12×18	H560×260×14×20	B650×650×26	H300×300×14×20	1.35
7	H590×240×12×18	H570×260×14×20	B650×650×26	H300×300×14×20	1.34
6	H600×240×12×18	H580×260×14×20	B700×700×30	H300×300×14×20	1.34
5	H610×240×12×18	H600×260×14×20	B700×700×30	H340×340×16×22	1.33
4	H620×240×12×18	H600×260×14×20	B800×800×30	H340×340×16×22	1.33
3	H620×240×12×18	H610×260×14×20	B800×800×30	H340×340×16×22	1.32
2	H630×240×12×18	H620×260×14×20	B850×850×30	H340×340×16×22	1.32
1	H630×240×12×18	H620×260×14×20	B850×850×30	H340×340×16×22	1.32

buildings under rare earthquakes. The FEMs of the analytical frame in all designs were established by SAP2000. Nominal yielding strength was adopted for the steel. The elastic modulus and Poisson's ratio are assumed to be 206,000 MPa and 0.3, respectively. The influence of initial imperfections and residual stress is not considered and P-delta effects were included in the nonlinear analyses. Nonlinear hinges were defined at the links, beams, columns, and braces.

5 Pushover Analysis

Pushover (static) analysis was performed through inverted triangular displacement-controlled patterns. In the pushover analysis, target drift selected 3% of the total height (D/H = 3%, D and H are the top displacement and total height of structure) of the frame. The lateral resistance capacities of all buildings were investigated through the nonlinear pushover analysis.

The ultimate deformation states and pushover curves of EBFs with different link lengths are shown in Figs. 28 and 29. Links in the inner height of the structures are firstly yielding to dissipate energy, and then the other links deformed to inelastic rotation. The same models with different link length have similar property and failure mode, later, the end of beams flexural yielding. Final, the column base was raised plastic hinges to the ultimate state of the HSS–EBF structures.

The pushover curves have shown apparently two stages. One is the elastic line segment, all members are still in elastic, and no plastic hinge has been found, the yielding point is defined as the end of the flexible line. Therefore, the x-coordinate of this position is yielding drift. Another is the elastic–plastic line segment. The roof drifts increases more quickly than the base shear. The end of the curves is the ultimate point, corresponding to the failure mode as shown in Fig. 28, and the x-coordinate value of this position is ultimate drift, and the ductility factor is the ultimate drift divided by yielding drift.

With the increase of link length, the yielding base shear force and ultimate bearing capacity of the structure gradually decreased, and the ductility and ultimate drift are steadily growing, because in the PBPD method, with the ductility demand increased, the design requirements need more considerable design base shear and more significant member sections. The yielding and ultimate data of the structures are summarized in Table 21. The yielding and ultimate base shear is reduced and ductility is raised with the link length increase. The same storey models with different link length have similar yielding drift while the ultimate drifts are different. Therefore, the yielding drift of HSS–EBF structure has not related to link length, and the ductility of HSS–EBF structure has significant with link length. When $e = 0$, the structure has no links, it is changed to the concentrically braced steel frame; the ductility is lower due to braces are buckling easily. When $e = L$ (the length of the span), the structure has no braces, it is changed to the moment-resisting steel frames, and the ductility has been improved because of the beam flexural yielding.

6 Time History Analysis

6.1 Ground Motion Records

All models were subjected to nonlinear dynamic analysis with various ground motions to study the deformation performance of the HSS–EBF structures under rare earthquakes. The dynamic analysis was performed using a set of ground motions. The seismological properties of the ground motions are summarized in Table 22, which also shows that rare earthquake level of seismic hazard was employed: 2% probability of exceedance in a 50-year period. The hypocentral distances range (R in Table 22) from the sources between 1.0 km (NGA0181) and 32.0 km for the earthquake records (NGA0292). Therefore, the above suite of strong motions covers well-defined design scenarios, include near and far-field conditions. The acceleration response spectra of the ensemble of accelerograms, along with the design acceleration spectrum are shown in Fig. 30.

Rare earthquake structural performance level, namely, collapse prevention limit states, is considered for the system assessment carried out in the present study. This limit state complies with seismic suggestions by FEMA 356 (2000).

6.2 Global Deformations

The mean maximum interstorey drifts for the structures during the earthquakes with probability exceedance of 2% are shown in Fig. 31, which reveals that the interstory drifts of

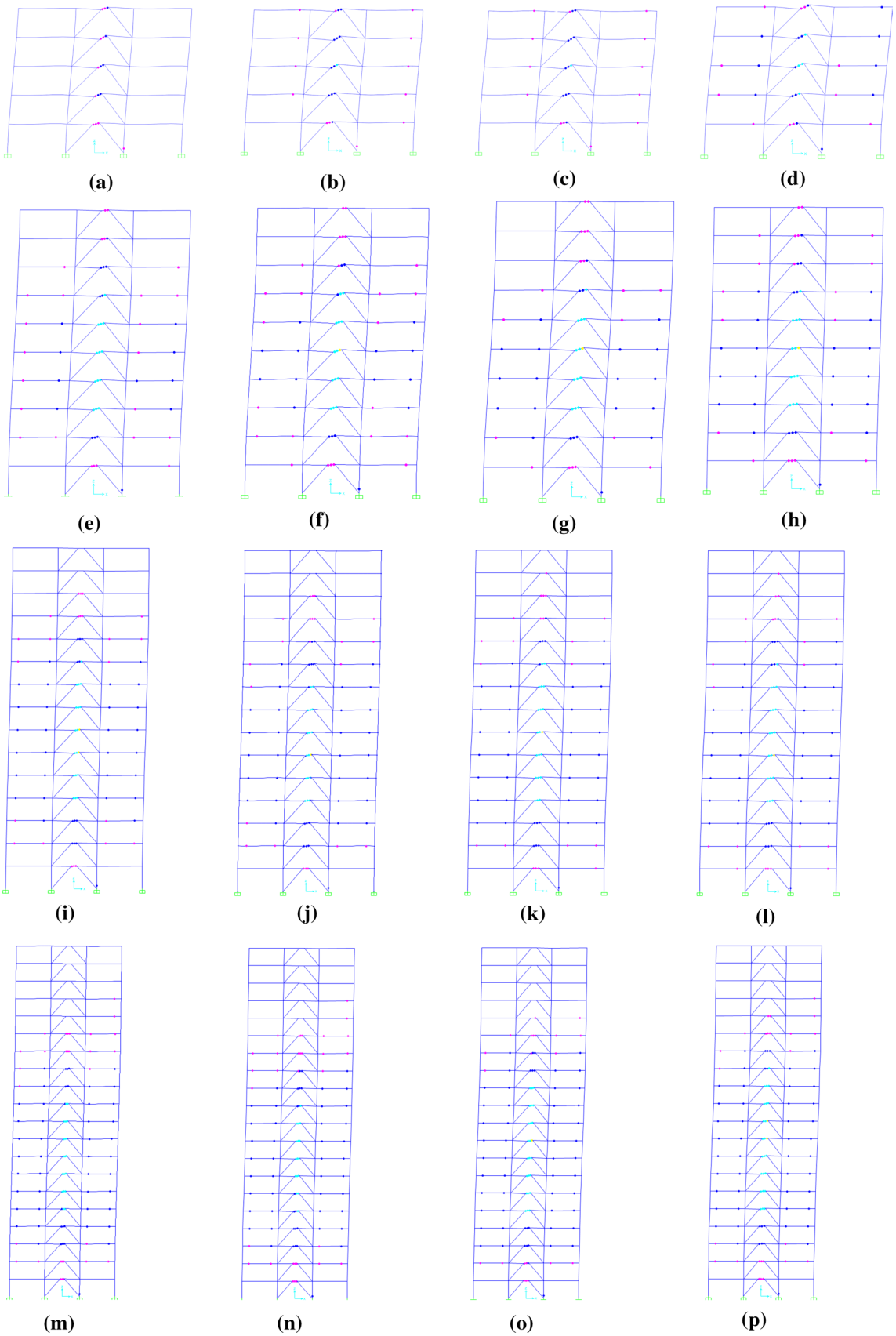
(a)
(b)
(c)
(d)
(e)
(f)
(g)
(h)
(i)
(j)
(k)
(l)
(m)
(n)
(o)
(p)

◂**Fig. 28** The ultimate deformation states of all models. **a** 5 storey with e = 900, **b** 5 storey with e = 1000, **c** 5 storey with e = 1100, **d** 5 storey with e = 1200, **e** 10 storey with e = 900, **f** 10 storey with e = 1000, **g** 10 storey with e = 1100, **h** 10 storey with e = 1200, **i** 15 storey with e = 900, **j** 15 storey with e = 1000, **k** 15 storey with e = 1100, **l** 15 storey with e = 1200, **m** 20 storey with e = 900, **n** 20 storey with e = 1000, **o** 20 storey with e = 1100, **p** 20 storey with e = 1200

all models are below the "Collapse prevention" limit (2%) in all cases. The mean maximum link rotations of models are presented in Fig. 32 as well, which shows that the link rotations of all models are below "Collapse prevention" limit (0.08 rad) in all cases. The storey drifts and link rotations indicated that the deformation distribution among the height of structure with different link length is similar to each other under rare earthquakes, though the member sections of HSS–EBFs are various due to PBPD method. The interstorey drifts and link rotations are raised with the increase of the link length, because of the lateral stiffness of the structures are decreased according to member sections.

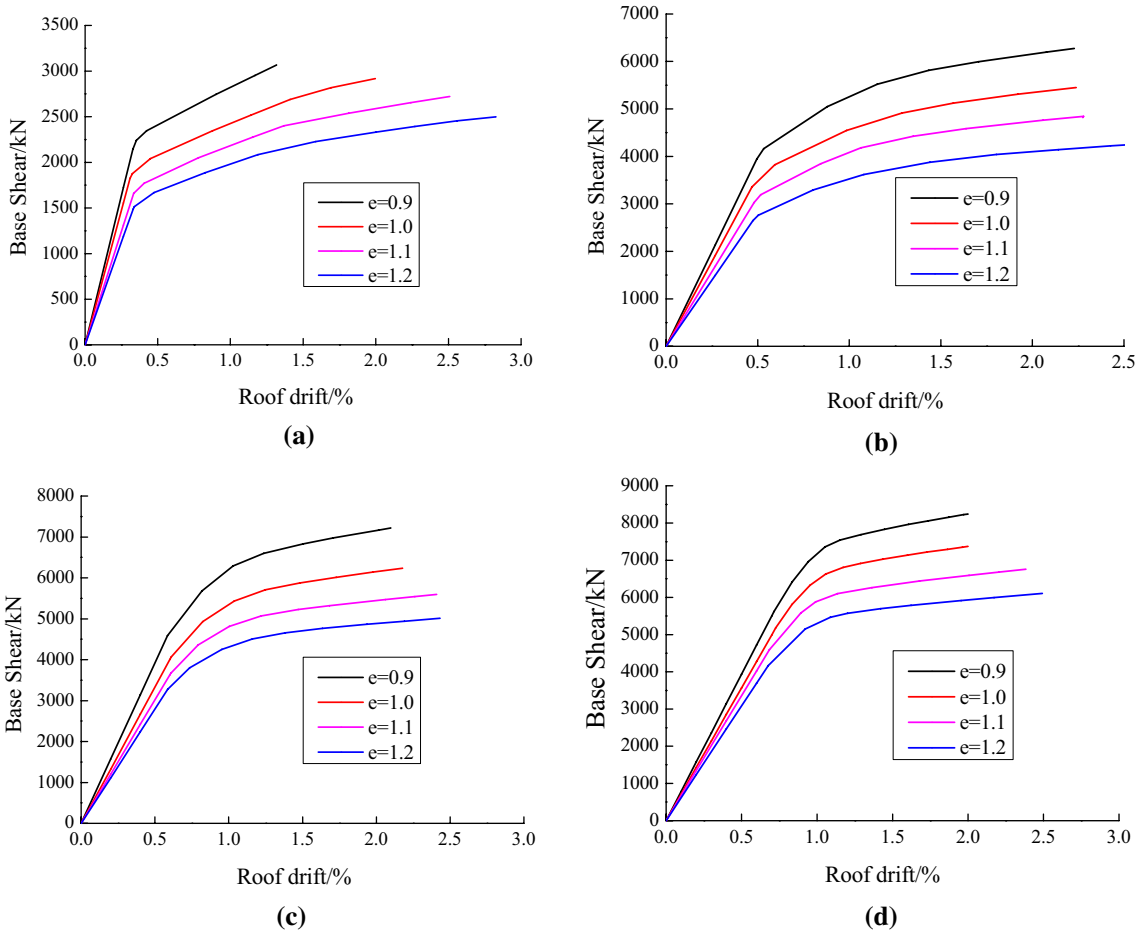

Fig. 29 Pushover curves. **a** 5 storey, **b** 10 storey, **c** 15 storey, **d** 20 storey

Table 21 The performance data of the structures

Structure	e (mm)	Yielding base shear (kN)	Yielding drift (%)	Ultimate base shear (kN)	Ultimate drift (%)	Ductility
5-storey	900	2240	0.35	3065	1.32	3.77
	1000	1874	0.33	2917	2.00	6.06
	1100	1600	0.33	2722	2.51	7.61
	1200	1515	0.34	2498	2.83	8.32
10-storey	900	4165	0.53	6273	2.23	4.21
	1000	3354	0.51	5452	2.24	4.39
	1100	3191	0.52	4818	2.30	4.42
	1200	2763	0.50	4243	2.51	5.02
15-storey	900	4587	0.58	7217	2.10	3.62
	1000	4068	0.59	6234	2.18	3.69
	1100	3669	0.61	5596	2.41	3.95
	1200	3274	0.59	5012	2.43	4.12
20-storey	900	5622	0.71	8243	2.00	2.82
	1000	5182	0.69	7372	2.00	2.90
	1100	4597	0.68	6757	2.38	3.50
	1200	4168	0.68	6106	2.49	3.66

Table 22 Ground motion records

Serial Number	Coding	Earthquake event	Recording stations	*M*	*R*/km	PGA_{max}/g	PGV_{max}/(cm/s)
1	NGA0829	Cape Mendocino 1992/04/25 18:06	89324 Rio Dell Overpass—FF	7.0	14.30	0.549	42.1
2	NGA0727	Superstitn Hills (B) 1987/11/24 13:16	01335 El Centro Imp. Co. Cent	6.5	5.60	0.894	42.2
3	NGA0802	Loma Prieta 1989/10/18 00:05	58065 Saratoga—Aloha Ave	6.9	13.0	0.324	41.2
4	NGA1485	Chi–Chi, Taiwan 1999/09/20	TCU045	7.6	24.1	0.512	39.0
5	NGA0068	San Fernando 1971/02/09 14:00	135 LA—Hollywood Stor Lot	6.6	21.2	0.210	18.9
6	NGA0821	Erzincan, Turkey 1992/03/13	95 Erzincan	6.9	2.0	0.496	64.3
7	NGA1605	Duzce, Turkey 1999/11/12	Duzce	7.1	8.2	0.535	83.5
8	NGA0292	Irpinia, Italy 1980/11/23 19:34	Sturno	6.5	32.0	0.358	52.7
9	NGA0181	Imperial Valley 1979/10/15 23:16	942 El Centro Array #6	6.5	1.0	0.439	109.8
10	NGA0960	Northridge 1994/01/17 12:31	90057 Canyon Country—W Lost Cany	6.7	13.0	0.482	45.1

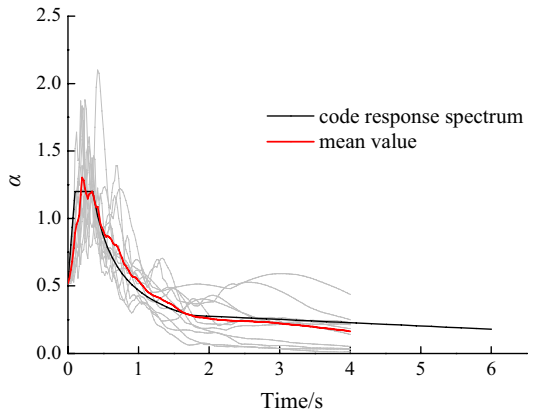

Fig. 30 Design spectra and scaled earthquake spectra

The failure modes of all buildings under rare earthquake are shown in Fig. 33. The failure modes show that links are primarily involved dissipate energy, the HSS–EBF models with different link length has the similar plastic hinge distribution. In 5-storey and 10-storey samples, all links yielding with other members still in elastic, while in 15-storey and 20-storey models, a few beam flexural yielding to dissipate energy due to the influence of high order mode.

7 Conclusion

Four groups of K-HSS-EBFs are successfully fabricated in this work, which includes 5-storey, 10-storey, 15-storey and 20-storey,and each group contain four different link length

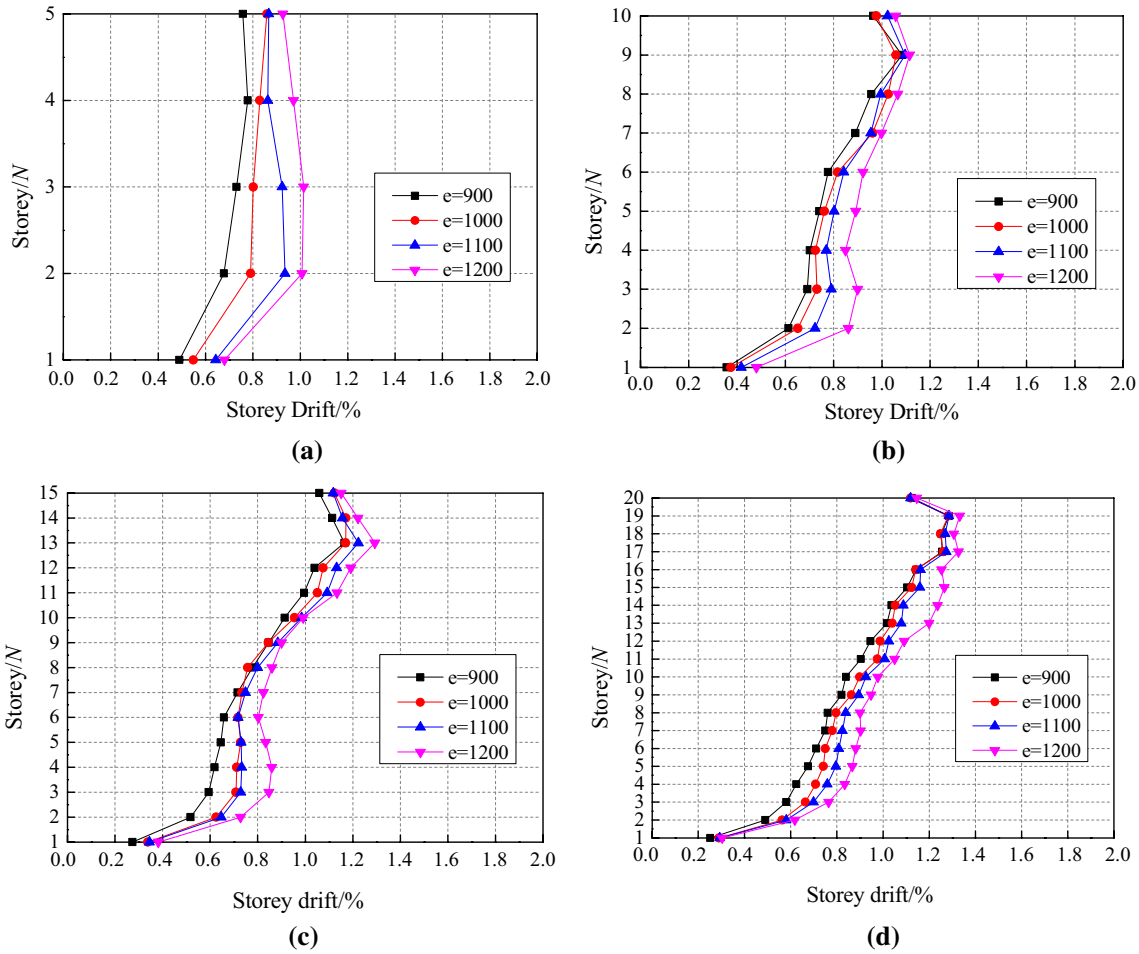

Fig. 31 Storey drifts under rare earthquake. **a** 5 storey, **b** 10 storey, **c** 15 storey, **d** 20 storey

(900, 1000, 1100 and 1200 mm). In the K-HSS–EBF, the link was made of Q345 steel with a nominal yield strength of 345 MPa, and the other structural members were made of Q460 steel with a nominal yield strength of 460 MPa. The links experience inelastic rotations while other components remained in elastic. Hence, the K-HSS–EBF is a reliable dual system.

The hysteretic behavior and performance of the K-HSS-EBF specimen with one-bay and three-storey was studied by using the cyclic test, including the failure mode, load-bearing capacity, ductility capacity, and energy dissipation capacity. The hysteretic curve shows the real plastic deformation capacity of the K-HSS–EBF. The K-HSS–EBF possessed stable and expanded hysteretic loops with no deterioration in the stiffness and load-bearing capacity. The hysteretic loops were very full, and it could be inferred that the K-HSS-EBF had a significant energy dissipation capacity. The test specimen failed because of the fracture of the link web on the second storey, and the link rotation capacity limits the ductility of the HSS–EBFs. The details should be

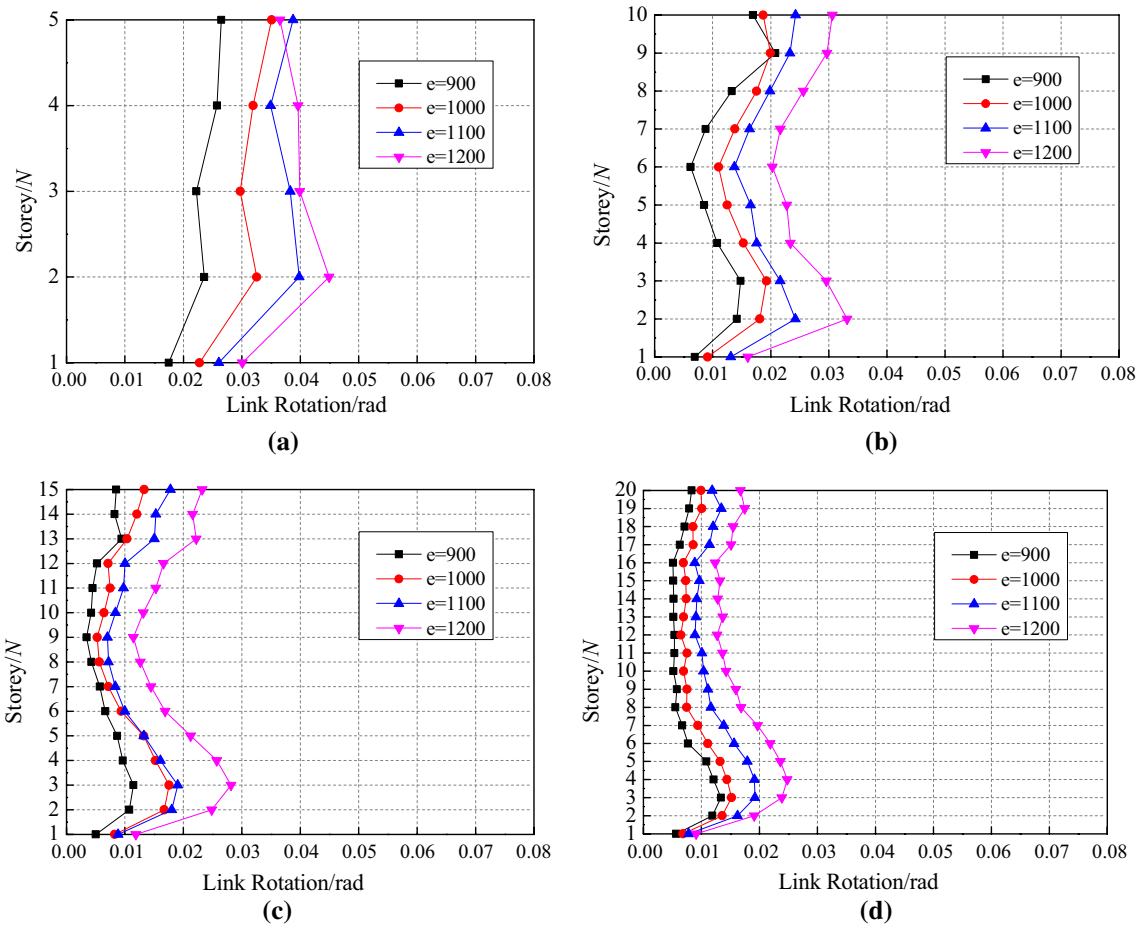

Fig. 32 Link rotations under rare earthquake. **a** 5 storey, **b** 10 storey, **c** 15 storey, **d** 20 storey

designed by no shear studs around the links to avoid composite action, and the connection location of link to beam should be outside of the link length to prevent the shear and moment at the end of links.

Also, the pushover and time history analysis were performed to study the seismic responses of the K-HSS–EBF models, including the static and dynamic properties, displacement responses, and failure mechanism. According to the distribution of the yielding locations, the plastic hinges located the positions of the link, beam end, and column base in the K-HSS-EBF when the structure reached the ultimate state. The ductility is increased with the link length increasing. As a result, the length (e) of link or the ratio e/L should be designed sufficiently large for excellent ductility under the allowed of architectural space, and the length ratio $\rho = eV_p/M_p$ of the shear link should be less than 1.6. The designed shear link dissipated the energy via shear deformation during the seismic loads. The link rotation and storey drift of the K-HSS–EBFs were increased with the link length increasing, the maximum link plastic rotation was less than

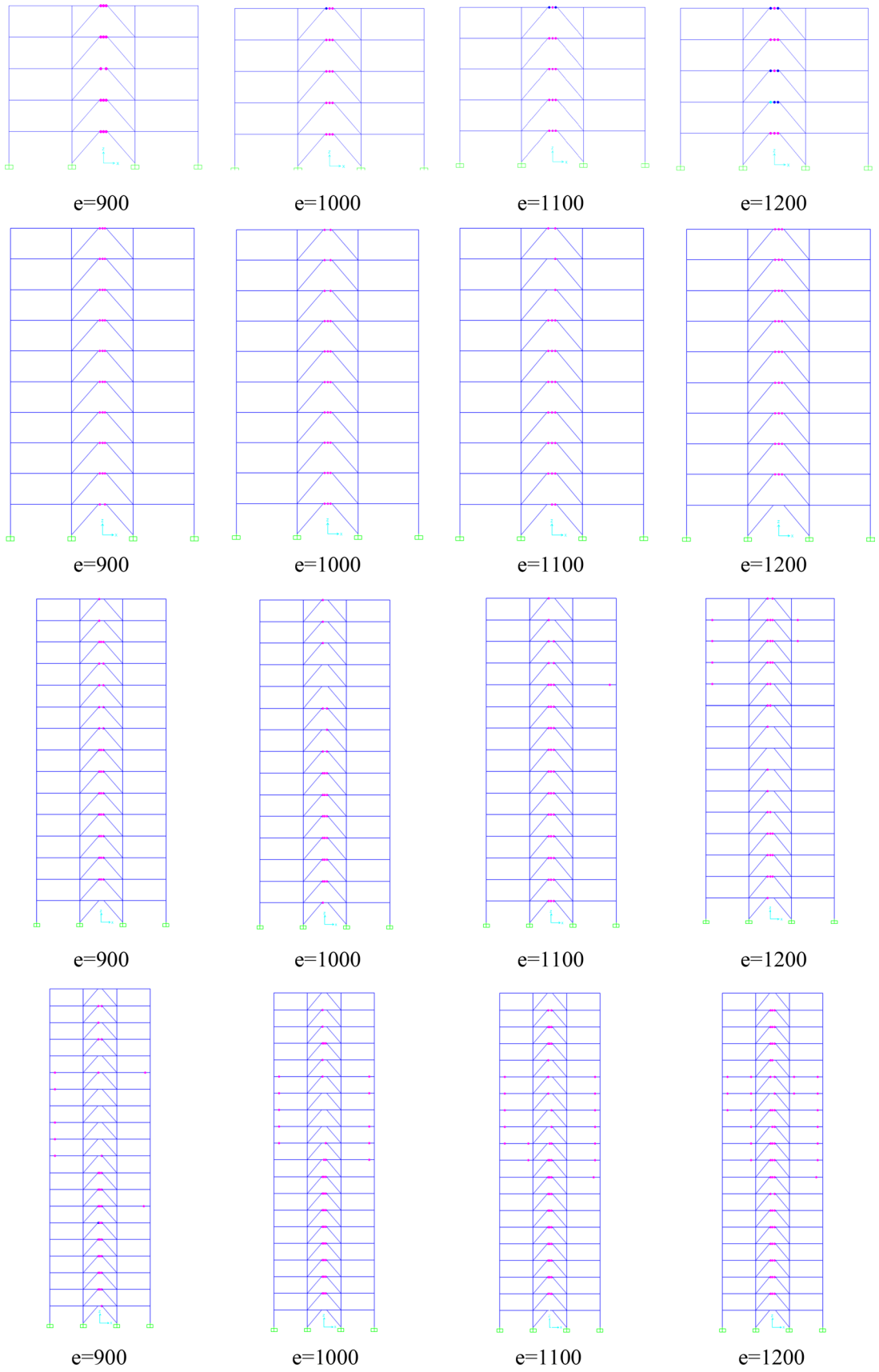

Fig. 33 Failure mode

0.08 rad for the shear link under rare earthquakes for all models, the storey drift was less than 2% as well.

Acknowledgements The authors are grateful for the financial support by the National Natural Science Foundation of China (Grant No. 51608441) and the Science Research Program of Shaanxi Educational Committee (Grant No. 17JK0542).

References

American institute of steel construction. (2010). AISC341-10 Seismic provision for structure steel buildings. Chicago, USA.

Azizinamimi, A., & Barth, K. (2004). High performance steel: Research front—historical account of research activities. *Journal of Bridge Engineering, 9*(3), 212–217.

Bosco, M., & Rossi, P. P. (2009). Seismic behaviour of eccentrically braced frames. *Engineering Structures, 31*(3), 664–674.

Chao, S. H., & Goel, S. C. (2014). Performance-based seismic design of EBF using target drift and yield mechanism as performance criteria. *Advances in Structural Engineering, 43*(4), 529–542.

Dubina, D., Stratan, A., & Dinu, F. (2008). Dual high-strength steel eccentrically braced frames with removable links. *Earthquake Engineering and Structural Dynamics, 37*(15), 1703–1720.

Dusicka, P., Itani, A., & Buckle, I. (2010). Cyclic behavior of shear links of various grades of plate steel. *Journal of the Structural Engineering, 136*(4), 370–378.

Federal emergency management agency. (2000). FEMA356 Prestandard and commentary for the seismic rehabilitation of buildings. Washington, DC, USA.

Green, P. S., Sause, R., & Ricles, J. M. (2002). Strength and ductility of HPS flexural members. *Journal of Constructional Steel Research, 58*(6), 907–941.

Hjelmstad, K. D., & Popov, E. P. (1982). Characteristics of eccentrically braced frames. *Journal of the Structural Engineering, 110*(2), 340–353.

Lian, M., Su, M. Z., & Guo, Y. (2015). Seismic performance of eccentrically braced frames with high strength steel combination. *Steel and Composite Structures, 18*(6), 1517–1539.

Mahin, S. A., & Shing, P. B. (1985). Pseudo dynamic method for seismic performance testing. *Structure Engineering, ASCE, 111*(ST7), 1482–1503.

Mans, P., Yakel, J., & Azizinamimi, A. (2001). Full scale testing of composite plate girders constructed using 485 MPa high performance steel. *Journal of Bridge Engineering, 6*(6), 598–604.

Ministry of Construction of the P.R.China. (2003). GB50017-2003 Code for design of steel structures. Beijing, China.

Ministry of Construction of the P.R.China. (2010). GB50011-2010 Code for seismic design of buildings. Beijing, China.

Okampto, S. et al. (1983). Techniques for large scale testing at BRI large scale structure test laboratory. *BRI Research Paper 101*, Ministry of Construction, Tsukuba, Japan.

Park, R. (1988). Ductility evaluation from laboratory and analytical testing. *Proceedings of ninth world conference on earthquake engineering* (pp. 605–616). Tokyo, Japan.

Speicher, M. S., & Iii, J. L. H. (2016). Collapse prevention seismic performance assessment of new eccentrically braced frames using ASCE 41. *Engineering Structures, 117*(6), 344–357.

Wang, F., Su, M. Z., Hong, M., et al. (2016). Cyclic behaviour of Y-shaped eccentrically braced frames fabricated with high-strength steel composite. *Journal of Constructional Steel Research, 120*(2), 176–187.